ClpP-dependent protein quality control supports antibiotic persistence in *Campylobacter jejuni* through bioenergetic homeostasis

Jinsong Feng[1,2,3#], Shenmiao Li[4#], Yaxi Hu[1&], Martin Stahl[5Ω], Lina Ma[1,2], Katelyn Knuff-Janzen[2], Kaidi Wang[4^], Yihan He[4], Bruce A. Vallance[5], Michael E. Konkel[6], B. Brett Finlay[2], Xiaonan Lu[1,4*]

[1] Food, Nutrition, and Health Program, Faculty of Land and Food Systems, The University of British Columbia, Vancouver, British Columbia, V6T 1Z4, Canada
[2] Michael Smith Laboratories, The University of British Columbia, Vancouver, British Columbia, V6T 1Z4, Canada
[3] Department of Food Science and Nutrition, Zhejiang University, Hangzhou, Zhejiang, 310058, China
[4] Department of Food Science and Agricultural Chemistry, Faculty of Agricultural and Environmental Sciences, McGill University, Sainte-Anne-de-Bellevue, Quebec, H9X 3V9, Canada
[5] British Columbia Children's Hospital Research Institute, Vancouver, British Columbia, V6H 3V4, Canada
[6] School of Molecular Biosciences, College of Veterinary Medicine, Washington State University, Pullman, WA 99164, USA

[#] Denoted as equal contribution
[*] Corresponding author. xiaonan.lu@mcgill.ca

[&] Current address: Food Science Program, Department of Chemistry, Carleton University, Ottawa, Ontario, K1S 5B6, Canada
[^] Current address: Department of Food and Bioproduct Sciences, University of Saskatchewan, Saskatoon, Saskatchewan, S7N 5A8, Canada
[Ω] Current address: STEMCELL Technologies Ltd, Vancouver, BC V6A 1B6, Canada.

ABSTRACT

Bacterial persistence enables survival during lethal antibiotic exposure and is implicated in recurrent infections, yet the physiology underlying bacterial persistence in many pathogens remains poorly defined. Here we show that exposure of *Campylobacter jejuni* to ampicillin or ciprofloxacin generates an antibiotic-persistent subpopulation. Rather than undergoing global metabolic shutdown, persister cells adopted a metabolically constrained state characterized by selective maintenance of oxidative phosphorylation and bioenergetic metabolism through coordinated proteostasis control. The ATP-dependent protease ClpP was essential for entry into this persistent state. Loss of ClpP disrupted proteostasis of the electron transport chain, specifically impaired *bd*-like terminal oxidase integrity, and reduced survival *in vivo* and in macrophages. These findings identify ClpP-dependent maintenance of redox and bioenergetic homeostasis as critical determinants of *C. jejuni* persistence and highlight metabolic remodeling as a defining feature of antibiotic tolerance. These insights may inform future therapeutic strategies aimed at disrupting persistence and improving antibiotic efficacy.

INTRODUCTION

Since Bigger's original observations, antibiotic persistence has been recognized as a phenotypic and non-heritable survival strategy by which a small subpopulation of bacteria survives otherwise lethal antibiotic exposure; these cells are termed persisters [1, 2]. Persisters have since been documented across diverse bacterial species and increasingly associated with the recalcitrance and relapse of bacterial infections [3-5]. Persistence is now recognized as a manifestation of phenotypic heterogeneity associated with variations in growth rate and adaptive physiological states, rather than a genetically encoded resistance phenotype [6-9].

Accumulating evidence suggests that bacterial metabolic state plays a central role in antibiotic tolerance. Bioenergetic and redox homeostasis underpin respiration, energy conservation, and metabolic processes required for growth and stress adaptation [10-12]. Bactericidal antibiotics disrupt essential cellular functions and often trigger energy-demanding compensatory responses, while numerous studies indicate that metabolic state both reflects and influences antibiotic lethality and survival [12-16]. Persister formation has frequently been associated with slowed growth, reduced biosynthetic activity, and low-energy states, but these features are increasingly viewed as part of a continuum of adaptive physiological states, rather than a binary switch between active and dormant cells [2, 17-19]. ATP depletion has been linked to increased survival during antibiotic challenge in *Staphylococcus aureus* and *Escherichia coli*, and their metabolic state can predict antibiotic lethality more accurately than growth rate, when growth and metabolism are experimentally uncoupled [8, 18-20].

Metabolic perturbation is also closely connected to protein homeostasis. ATP depletion has been linked to protein aggregation and persistence-associated dormancy [21, 22]. In bacteria, protein aggregation arises from proteostatic stress and has been associated with altered growth, loss of protein function, stress tolerance, and pathogenicity [22-25]. Deletion of *pspA* in stationary-phase *E. coli* lowers intracellular ATP levels, accelerates protein aggregation, and increases persistence, whereas glucose supplementation partially restores ATP levels and reduces persister formation [26]. ATP-dependent protein aggregation has also been shown to correlate with dormancy depth and lag time, while the DnaK–ClpB disaggregation machinery is required for efficient resuscitation [22]. These findings suggest that protein aggregation may link bioenergetic stress, slowed growth, dormancy depth, and antibiotic survival.

Proteostasis has also been implicated in toxin–antitoxin (TA) models of persistence, in which antitoxin degradation and toxin activation were proposed to promote reversible growth arrest [27]. In *E. coli*, MazF-mediated persistence was reported to require the ClpP and Lon proteases [28]. However, the broader contribution of type II TA systems to antibiotic persistence remains debated, as deletion of ten chromosomal type II TA loci in *E. coli* did not impair persistence to ampicillin or ofloxacin [29]. Still, individual toxins can influence persistence-associated physiology. For example, the SOS-regulated type I membrane toxin TisB promoted dormancy-

linked changes, including dissipation of the proton motive force, loss of pH homeostasis, and in some contexts, protein aggregation that prolongs dormancy [30, 31].

In parallel, studies of bactericidal antibiotic lethality proposed a shared oxidative death pathway mediated by reactive oxygen species (ROS) [16]. Although influential, this model has been recently revised, as subsequent work demonstrated that bactericidal activity can occur independently of ROS and under oxygen-limited conditions [32, 33]. The field now recognizes that antibiotic stress perturbs respiration, electron flow, and cellular redox physiology in a context-dependent manner, with ROS representing one possible downstream consequence rather than a universal mechanism [8, 34-36]. From this perspective, redox imbalance provides a more robust lens through which to understand how antibiotic stress reshapes bacterial physiology and survival.

These questions are particularly relevant in *Campylobacter jejuni*, a leading cause of foodborne bacterial gastroenteritis worldwide. Compared with many bacterial pathogens, *C. jejuni* has a relatively small genome (~1.6–1.7 Mb) and lacks several classical stress-response regulators, including RpoS, OxyR, and SoxRS [37, 38]. Despite these apparent limitations, *C. jejuni* survives diverse environmental and host-associated stresses and can form antibiotic-tolerant persisters. A clinical case study described relapsing infections associated with long-term colonization despite antibiotic treatment [4], and additional studies showed that exposure to antibiotics, such as ciprofloxacin, penicillin G, or tetracycline can generate tolerant or persister-like subpopulations [39-41]. In penicillin G-treated cells, Morcrette and co-authors identified a subpopulation of *C. jejuni* with increased fluorescence after staining with a redox-sensitive dye, suggesting altered redox activity or respiratory remodeling [40]. Nevertheless, the physiological mechanisms underlying the persistence in *C. jejuni* remain poorly defined.

Here, we investigated how metabolic adaptation supports antibiotic persistence in *C. jejuni*, with a particular focus on the coupling between redox homeostasis, bioenergetic remodeling, and proteostasis. Using antibiotics with strong metabolic dependencies, together with genetic, physiological, and metabolic analyses, we investigated whether persistence reflects generalized metabolic suppression or instead a more selective remodeling of survival-associated pathways. Our findings identify ClpP-dependent proteostasis as a central determinant of antibiotic tolerance and suggest that antibiotic-tolerant *C. jejuni* undergoes respiratory and redox remodeling rather than a uniform metabolic shutdown.

RESULTS

C. jejuni forms an antibiotic-tolerant subpopulation with bactericidal antibiotic treatment

To determine whether *C. jejuni* can develop antibiotic tolerance when exposed to bactericidal antibiotics with distinct primary targets, we performed time-killing assays using ampicillin and ciprofloxacin in four representative *C. jejuni* strains (F38011, 81-116, 87-95, 11168) with slightly

118 different genetic backgrounds. Under antibiotic concentrations that were bactericidal, we
119 observed marked heterogeneity within the *C. jejuni* populations. Although most cells were
120 rapidly eliminated, a small surviving fraction exhibited a substantially slower killing rate,
121 resulting in a biphasic killing pattern (**Fig. 1a, b**). This biphasic pattern was consistently
122 observed across all four strains tested, indicating that persister formation was not limited to a
123 single strain background in our strain set. To exclude the possibility that the surviving cells
124 represented transiently resistant variants, we repeatedly challenged the survivors with the same
125 antibiotics over four successive rounds. No increase in MIC was detected, indicating that the
126 surviving subpopulation had not acquired heritable resistance (**Extended Data Figure 1** and
127 **Supplementary Table 1**). We also ruled out the possibility that reduced killing at later time
128 points resulted from antibiotic degradation by pre-incubating the antibiotics under the same
129 conditions used in the killing assays for 6 h prior to bacterial exposure. This pre-incubation did
130 not alter the MICs of either antibiotic. Collectively, these results demonstrated that *C. jejuni*
131 transiently formed an antibiotic-tolerant subpopulation under bactericidal antibiotic stress, and
132 that the survival of this subpopulation reflected physiological adaptation, rather than stable
133 resistance mutations.

134 **Multi-omics profiling reveals proteostasis and respiratory remodeling in tolerant cells**

135 To characterize the physiological state of antibiotic-tolerant *C. jejuni* cells, we performed
136 transcriptomic and proteomic analyses on the tolerant fraction collected after ampicillin or
137 ciprofloxacin treatment. Gene set enrichment analysis of the transcriptomic data revealed
138 consistent enrichment of pathways associated with protein catabolism and quality control, SOS
139 and stringent stress responses, peptidoglycan synthesis, and RNA processing. In contrast,
140 pathways related to flagellum-dependent motility, the TCA cycle, and respiration/electron
141 transport were under-represented (**Fig. 1f**). These results indicate that antibiotic-tolerant cells do
142 not simply undergo global metabolic shutdown, instead they adopted a selective regulatory
143 program characterized by enhanced stress adaptation and altered respiratory activity. Proteomic
144 profiling further supported this interpretation, indicating preservation of stress and homeostasis-
145 associated functions despite broad metabolic restriction. Although transcriptomic and proteomic
146 changes were not fully concordant, several key functional trends were consistent across both
147 datasets. Notably, pathways involved in protein folding and quality control remained enriched
148 under both antibiotic treatments, suggesting sustained investment in proteostasis despite the
149 energetically restricted state of tolerant cells. Ciprofloxacin exposure induced broader proteomic
150 changes than ampicillin, yet both treatments converged on a shared signature involving protein
151 homeostasis and metabolic reprogramming.

152 **ClpP is critical for antibiotic tolerance in *C. jejuni***

153 To investigate the pathways involved in antibiotic tolerance, we generated a panel of *C. jejuni*
154 mutants on the F38011 background, including mutants defective in the stringent response
155 (Δ*spoT*) [42], SOS response (Δ*recA*) [43], and ATP-dependent proteolysis (Δ*lon* and Δ*clpP*) [44].
156 We then compared their survival under ampicillin and ciprofloxacin treatment (**Fig. 1c, d**).

157 Primers and plasmids used for strain construction are listed in **Supplementary Table 2**. Deletion
158 of *spoT* or *recA* did not affect tolerance to ampicillin, whereas deletion of *recA* selectively
159 reduced survival under ciprofloxacin treatment, consistent with the established role of RecA in
160 DNA damage repair. In contrast, deletion of *clpP* markedly compromised survival under both
161 ampicillin and ciprofloxacin treatment, while deletion of *lon* had no significant effect under
162 either antibiotic condition. Importantly, the Δ*clpP* mutant displayed MIC values comparable to
163 those of the wild-type strain and showed no significant growth defect under non-stressed
164 conditions. Therefore, the reduced survival of the Δ*clpP* mutant cannot be attributed to altered
165 intrinsic susceptibility or impaired growth but instead reflects a specific defect in antibiotic
166 tolerance. Collectively, these results identify ClpP as a key determinant of antibiotic tolerance in
167 *C. jejuni*.

168 ***clpP*-associated protein regulation links tolerance to respiratory homeostasis**

169 To further refine the *clpP*-associated regulatory module, we stratified proteins according to their
170 abundance correlation with *clpP* and their predicted disorder tendency. The *clpP*-centered protein
171 co-expression analysis identified 241 proteins whose abundance was strongly correlated with
172 *clpP* expression (absolute Pearson correlation coefficient > 0.8, $p < 0.05$; **Supplementary Table**
173 **3**). These proteins were predominantly associated with pathways related to 1) energy production
174 and conversion, 2) amino acid transport and metabolism, 3) translation, ribosomal structure, and
175 biogenesis, 4) cell wall, membrane and envelope biogenesis, and 5) post-translational
176 modification, protein turnover, and chaperones (**Fig. 1e**). These *clpP*-correlated proteins were
177 overall better maintained during antibiotic treatment than non-correlated proteins, showing
178 higher relative abundance under both ampicillin and ciprofloxacin exposure (**Fig. 2a, b**). We then
179 analyzed the disorder tendency of the *clpP*-correlated proteins using DFLpred [45] and classified
180 them into high-, medium-, and low-disorder groups. This stratification was used to determine
181 whether the ClpP-associated module was preferentially linked to proteins with greater predicted
182 structural flexibility, given that proteins with elevated aggregation risk are often subject to tighter
183 transcriptional, translational and degradation control as part of cellular proteostasis strategies
184 [46]. Among the *clpP*-correlated proteins detected in both conditions, 83 were classified as high-
185 disorder, 135 as medium-disorder, and 22 as low-disorder (**Fig. 2c, d**; **Table S3**). In contrast,
186 among the 132 low-disorder proteins detected, only 22 were *clpP*-correlated whereas 110 were
187 non-correlated, indicating that ClpP-associated regulation was preferentially linked to proteins
188 with higher disorder tendency. Consistently, the high-disorder subset showed the highest relative
189 abundance within the *clpP*-correlated cluster under both antibiotic treatments (**Fig. 2c, d**).
190 Comparison of mRNA and protein fold changes for the *clpP*-correlated/high-disorder subset
191 further revealed an asymmetric transcript–protein relationship, in which positive mRNA changes
192 were more closely reflected at the protein level than negative mRNA changes (**Fig. 2e, f**).
193 Mapping these features onto KEGG pathways further showed that the *clpP*-correlated/high-
194 disorder module was associated with selectively maintained functions in
195 glycolysis/gluconeogenesis, pyruvate metabolism, the TCA cycle, oxidative phosphorylation,

196 and amino acid metabolism. In contrast, functions related to fatty acid elongation, biotin
197 biosynthesis, and parts of histidine, lysine, and glutamate metabolism were suppressed (**Fig. 2g**).

198 **ClpP supports the antibiotic-induced respiratory response and *bd*-like terminal oxidase**
199 **integrity**

200 Because multi-omics analysis pointed to substantial remodeling of respiration- and electron
201 transport-associated pathways, we next assessed respiratory activity by measuring the oxygen
202 consumption rate (OCR) using Seahorse analysis. Antibiotic exposure triggered a transient
203 increase in oxygen consumption, manifested as a distinct OCR peak (**Fig. 3a**). Notably, the wild-
204 type F38011 strain exhibited a stronger respiratory response than the Δ*clpP* mutant and
205 maintained higher overall respiratory activity throughout the post-treatment period.
206 Normalization of OCR to viable cell counts showed that antibiotic-treated wild-type cells still
207 exhibited higher respiratory activity than the Δ*clpP* mutant (**Fig. 3b**). Thus, the reduced OCR
208 observed in Δ*clpP* cannot be attributed solely to differences in viable cell number after treatment.
209 Rather, these data support a role for ClpP in maintaining bioenergetic homeostasis during
210 antibiotic stress.

211 *C. jejuni* encodes two terminal oxidases, the high-affinity cbb_3-type oxidase CcoNOQP and a
212 cyanide-insensitive *bd*-like oxidase encoded by *cydAB* (also referred to as *cioAB*) [47, 48].
213 Previous studies indicate that the cbb_3 branch is the major high-affinity oxidase supporting
214 microaerobic respiration, whereas the *bd*-like branch is a lower-affinity oxidase whose
215 expression increases under higher oxygen availability and is more commonly associated with
216 stress-adaptive respiration [48, 49]. Transcriptomic analysis further showed selective remodeling
217 of central metabolic and respiratory functions in antibiotic-treated cells. Selected TCA cycle
218 genes were downregulated, and the downregulated respiratory genes were primarily enriched in
219 oxidative phosphorylation and electron transport chain complex I, II, III, and IV (CcoNOQP). By
220 contrast, genes associated with ATP synthase complex V were upregulated (**Extended Data**
221 **Figure 2**). In addition, *cydAB* (*cj0081* and *cj0082*) was upregulated in both antibiotic-treated
222 populations (**Table S6, Extended Data Figure 2**). These patterns suggest altered respiratory
223 coupling, reduced proton-translocating respiratory capacity and sustained energetic demand.

224 We next examined the *bd*-like terminal oxidase subunit CydA by Western blotting following
225 exposure to antibiotics at MIC. Untreated controls displayed the characteristic CydA banding
226 pattern under unstressed conditions. At 30 min, CydA-associated signals were weak across
227 antibiotic-treated samples, limiting interpretation at this early time point (**Fig. 3c, left**). By 12 h,
228 a clearer difference emerged between strains. Specifically, wild-type cells displayed a
229 reproducible multi-band CydA pattern spanning approximately 65-75 kDa, including a major
230 upper band at ~75 kDa and several lower-molecular-weight bands between ~60 and 70 kDa. In
231 contrast, the Δ*clpP* mutant showed an altered pattern characterized by loss of the band at ~70
232 kDa, while retaining the major upper band (**Fig. 3c, right**). Because CydA is a membrane-
233 embedded subunit of the *bd*-like terminal oxidase, detection of multiple CydA-associated bands
234 is not unexpected, although the basis of these species remains unresolved. This shift in the CydA

235 banding pattern suggests that the respiratory defect in the Δ*clpP* mutant involves altered CydA-
236 associated terminal oxidase integrity rather than complete loss of the *bd*-like terminal oxidase.

237 **Antibiotic-tolerant cells undergo redox-linked metabolic and membrane lipid remodeling**

238 To further define the metabolic state of antibiotic-tolerant cells, we performed metabolomic and
239 lipidomic analyses to examine changes in both hydrophilic and hydrophobic metabolites (**Fig.**
240 **4a, d**, **Tables S4 and S5**). The metabolomic data collectively revealed an overall decrease in the
241 abundance of metabolites associated with core metabolic pathways. Consistent with the
242 regulatory patterns inferred from transcriptomics and proteomics, metabolites involved in biotin
243 biosynthesis and histidine, lysine, and glutamate metabolism were significantly downregulated
244 (**Fig. 4b, c** and **Figure S3**). Importantly, key metabolites involved in glycolysis, the TCA cycle,
245 and amino acid metabolism were also overtly depleted, indicating broad suppression of central
246 carbon metabolism. In contrast, several metabolites involved in nucleotide sugar metabolism and
247 the pentose phosphate pathway, including UDP-xylose, UDP-D-glucose, and UDP-glucuronate,
248 accumulated under both ampicillin and ciprofloxacin treatment. To further interpret this shift, we
249 constructed a core metabolic map of *C. jejuni* (**Fig. 5a**). This analysis suggested that the apparent
250 upregulation of glycolysis/gluconeogenesis-related reactions did not necessarily reflect increased
251 glycolytic flux, but rather a redirection of carbon toward nucleotide sugar metabolism. The
252 tolerant cells also displayed a shunted TCA cycle, depletion of the glutamate–glutamine cycle,
253 and accumulation of redox-associated metabolites such as S-adenosylmethionine, riboflavin-5-
254 phosphate, and menaquinone-6. Together, these findings support a metabolically constrained but
255 redox-oriented tolerant state.

256 Lipidomic analysis further revealed pronounced membrane remodeling in antibiotic-tolerant
257 cells. Fatty acids with chain lengths predominantly ranging from C_{14} to C_{18} accumulated under
258 both antibiotic treatments (**Fig. 4e, f**), whereas biotin, a cofactor required for fatty acid
259 biosynthesis, was significantly depleted (**Figure S3**), suggesting that fatty acid accumulation
260 primarily resulted from catabolic processes rather than de novo synthesis. In addition, a broad
261 range of lysophospholipids, particularly species with C_{16} and C_{18} chains, was significantly
262 enriched in tolerant cells. This was accompanied by upregulation of *pldA* (**Table S7**), which
263 encodes an outer membrane phospholipase that can hydrolyze oxidized phospholipids to
264 generate lysophospholipids and free fatty acids under stress conditions [50, 51]. Consistent with
265 this, oxidized phosphatidylethanolamine intermediates were also detected (**Figures S6** and **S7**),
266 suggesting that antibiotic treatment promoted phospholipid oxidation and lipid turnover even
267 though bulk lipid peroxidation was not markedly increased (**Figures S4** and **S5**). These lipid
268 changes indicated that the tolerant state is accompanied by membrane turnover and phospholipid
269 remodeling.

Loss of ClpP compromises redox homeostasis and host survival

Given the central role of ClpP in antibiotic tolerance and the extensive redox- and membrane-associated remodeling observed in tolerant cells, we next examined whether loss of ClpP disrupts homeostasis more broadly. Deletion of *clpP* increased sensitivity to oxidative stress and elevated lipid peroxidation, indicating that ClpP contributes to the maintenance of both redox balance and membrane integrity (**Fig. 4 and Figure S4**). This phenotype is consistent with a role for ClpP-dependent protein quality control in limiting damage accumulation under stress conditions, and in preserving processes linked to respiratory function. We then assessed whether this defect affected host-associated survival. In RAW 264.7 macrophages, the wild-type and Δ*clpP* mutant strains exhibited similar adherence at 3 h post-infection, but the Δ*clpP* mutant rapidly lost viability thereafter and became undetectable by 8 h post-infection (**Fig. 5b**). To further evaluate the pathogenic relevance of this phenotype *in vivo*, we infected Sigirr-deficient mice, which were previously shown to be susceptible to enteric *C. jejuni* infection [52], and measured intestinal pathogen burdens. As expected, Sigirr-deficient mice were heavily colonized by wildtype *C. jejuni* F38011. Although the Δ*clpP* mutant retained some colonization capacity, its bacterial load was significantly lower than that of the wild-type strain (**Fig. 5c**). Histological analysis further showed that wild-type cells formed microcolonies on the epithelial surface, whereas the Δ*clpP* mutant was only rarely detected at the intestinal surface (**Fig. 5d, e**). Taken together with the *in vitro* stress phenotypes, these results extended the role of ClpP from antibiotic tolerance to survival in host-associated environments.

DISCUSSION

Antibiotic tolerance has long been viewed as a stochastic survival phenomenon, but it is increasingly recognized as the outcome of coordinated physiological states that allow a subpopulation of bacterial cells to survive otherwise lethal antibiotic exposure [14, 53, 54]. This conceptual shift has also highlighted metabolism as a central determinant of antibiotic efficacy, tolerance, and the longer-term evolution of resistance [14, 53, 55]. Recent work further argues against viewing persistence simply as metabolic dormancy, instead emphasizing metabolically rewired and physiologically heterogeneous survival states [56]. Within this framework, our data support a view in which antibiotic tolerance in *C. jejuni* reflects active homeostatic remodeling rather than passive metabolic shutdown, with ClpP-dependent proteostasis emerging as a key feature of this state. This interpretation aligns with the broader role of ClpP in bacterial stress fitness, virulence, and proteome control across species, including *Listeria monocytogenes* and *Staphylococcus aureus* [57-60], and with mechanistic work showing that the ClpXP system can act on structurally diverse substrates through flexible recognition modes [61, 62]. It also aligns with growing interest in bacterial proteases as antimicrobial targets, including compounds that kill cells by dysregulating ClpP-mediated proteolysis [63].

Classical persistence-associated determinants include alarmone signaling, TA modules, stress-responsive proteases, and phenotypic switching networks [54, 64-66]. Our data suggest that

antibiotic tolerance in *C. jejuni* depends less on a single canonical persistence pathway and more on the capacity of the cell to maintain physiological integrity during stress. Among the mutants tested, only Δ*clpP* showed compromised survival under both ampicillin and ciprofloxacin treatment, whereas Δ*recA* showed a condition-specific defect matching DNA damage repair, while Δ*spoT* and Δ*lon* did not phenocopy the survival defect. Because deletion of *clpP* did not alter MIC or basal growth, its phenotype is most consistent with a specific defect in tolerant-state survival. Tolerant cells showed enrichment of protein quality control and damage repair functions alongside repression of multiple growth-associated processes [10, 14, 65, 67, 68]. The partial transcript-protein discordance is mechanistically informative rather than problematic. Proteome allocation is not dictated solely by transcript abundance [69, 70], and translational regulation can further shape protein output even when transcript changes are incomplete or transient [71]. Recent work in *C. jejuni* has also revealed a more complex translatome and a broader role for translation-level regulation [72]. Proteostasis vulnerabilities are highly condition-specific [73], and proteases can support survival during growth arrest in a hierarchical manner, with ClpXP often playing a more dominant and nonredundant role than Lon [64]. Small-molecule studies likewise emphasize the importance of ClpP in tolerance, as dysregulation or hyperactivation of ClpP can eliminate persister populations [74, 75]. The enrichment of protein quality control across both datasets and the preferential association of ClpP with structurally vulnerable proteins support a model in which ClpP helps preserve a selective homeostatic proteome under proteotoxic stress [25, 76, 77]. Because repair and clearance of damaged proteins are energetically costly, this model also implies that tolerant cells remain selectively active rather than passively shut down. This view is reinforced by biochemical and single-molecule evidence that AAA+ protease systems engage substrates probabilistically and through diverse recognition modes [61, 62].

Functionally, this ClpP-associated module was enriched in central metabolism, oxidative phosphorylation, and amino acid metabolism, linking proteostasis to respiratory homeostasis. Rather than pointing to separate defects, the Seahorse and Western blot data converge on the view that antibiotic challenge imposed a respiratory-redox transition and that ClpP was required to maintain homeostasis through that transition [10, 78-82]. Given that *C. jejuni* physiology is tightly shaped by oxygen availability and a branched electron transport chain [47, 48, 83], and prior evidence has linked ClpXP to oxidative stress responses, redox sensing, and aerobic-anaerobic transitions [61], our findings support a role for ClpP in maintaining bioenergetic stability during antibiotic challenge.

The metabolomic and lipidomic data further define the tolerant state as one shaped by redox-linked metabolic adaptation and membrane remodeling. Depletion of central carbon metabolites together with accumulation of selected nucleotide-sugar intermediates and redox-associated metabolites points to redirected carbon use and a redox-oriented survival physiology, in line with evidence that pentose phosphate metabolism and redox-active metabolites can shape antibiotic lethality and tolerance [10, 84]. In parallel, accumulation of fatty acids and lysophospholipids,

347 biotin depletion, *pldA* upregulation, and detection of oxidized phosphatidylethanolamine
348 intermediates indicate membrane turnover and phospholipid remodeling. Because the membrane
349 provides the structural platform for electron transport and proton translocation, these lipid
350 changes are likely relevant to respiratory homeostasis [85]. They may also influence host
351 interactions, given the emerging relevance of lysophosphatidylethanolamine in *C. jejuni*
352 virulence [86]. Loss of ClpP also increased oxidative stress sensitivity and lipid peroxidation and
353 reduced survival in macrophages and in the murine gut, indicating that ClpP-dependent functions
354 that support antibiotic survival also contribute to fitness in host-associated environments, in line
355 with prior work linking respiratory flexibility and niche adaptation in *Campylobacter* [47, 48,
356 83] and with evidence that ClpXP contributes to antioxidant control and population-level fitness
357 maintenance in *S. aureus* [60].

358 Our data support a model in which antibiotic-tolerant *C. jejuni* cells exist in a metabolically
359 constrained but selectively active state. We summarize this model in **Fig. 6**. Under basal
360 microaerobic conditions, respiration supports efficient energy conservation while ClpP-
361 dependent proteostasis maintains proteome integrity. Following bactericidal antibiotic exposure,
362 surviving cells transition into a stress-associated tolerant state characterized by respiratory
363 remodeling, redox-oriented metabolic adaptation, and increased reliance on protein quality
364 control. In this state, ClpP-mediated clearance of damaged proteins helps preserve cellular
365 homeostasis, and disruption of this proteostasis–respiration–redox axis sensitizes *C. jejuni* to
366 both antibiotic and host-derived stress [14, 54, 55, 64, 74, 75]. More broadly, some antibiotic-
367 tolerant states may depend less on passive shutdown than preservation of a minimal but critical
368 homeostatic core under stress, particularly where proteostasis, respiration, and redox balance are
369 tightly coupled. In this view, *C. jejuni* is informative because its reduced redundancy allows this
370 ClpP-dependent homeostatic core to be resolved more clearly. ClpP-dependent proteostasis
371 therefore emerges not simply as a species-specific determinant of tolerance, but as part of a
372 broader mechanism of bacterial stress survival and a potentially useful antimicrobial target.

373 MATERIALS AND METHODS

374 Bacterial strains and growth conditions

375 *C. jejuni* strain F38011 is a representative clinical isolate obtained from a fecal sample from a
376 patient with bloody diarrhea, and was used in the current study [87]. Three additional *C. jejuni*
377 strains 81116, 87-95, and 11168 were used in the antibiotic killing assay. Bacteria were routinely
378 cultivated either on Mueller-Hinton agar (MHA) or in Mueller-Hinton broth (MHB)
379 supplemented with selective antibiotics (chloramphenicol or kanamycin) at 37°C under
380 microaerobic conditions.
381

382 Construction of *C. jejuni* mutants and complementation

383 The mutants of *C. jejuni* F38011 were generated by replacing the genomic coding region of the
384 targeted gene with a drug resistance gene using homologous recombination. The sequences of

385 the primers are listed in **Table S1**. The *lon* deletion mutant was generated by homologous
386 recombination and insertion of a chloramphenicol resistance cassette (Cm^R). The upstream and
387 downstream regions flanking *lon* (*lon*^{up}, *lon*^{down}) were PCR-amplified using the primer pairs
388 OLU182/OLU183 and OLU186/OLU187, respectively. The Cm^R gene was amplified from the
389 plasmid pACYC184 using the primer pairs OLU184/OLU185. The above three PCR fragments
390 were purified using the Gel/PCR purification kit (Froggabio, CA) and inserted into EcoRI/XbaI-
391 digested pUC19 using the NEBuilder® HiFi DNA Assembly Cloning Kit. The plasmid pUC19-
392 *lon*^{up}-*Cm*^{R}-*lon*^{down} was introduced into *C. jejuni* strain F38011 via natural transformation.
393 Transformants were selected on MHA supplemented with 2 µg/mL Cm (MHBCm2) and streaked
394 on the MHACm8 agar to confirm Cm resistance. Deletion of *lon* was confirmed by PCR.
395
396 The *clpP* deletion mutant of *C. jejuni* was generated using a similar protocol as described above.
397 Briefly, upstream and downstream regions flanking *clpP* (*clpP*^{up}, *clpP*^{down}) were PCR-amplified
398 using the primer pairs OUL196/OLU197 and OLU200/OLU201, respectively. The Cm^R gene
399 was amplified from pACYC184 using the primer pair OLU198/OLU199. The engineered
400 plasmid pUC19-*clpP*^{up}-*Cm*^{R}-*clpP*^{down} was transformed into *C. jejuni* strain F38011, followed by
401 selection on the MHACm2 and MHACm8 agar, subsequently. Deletion of *clpP* was confirmed
402 by PCR.
403
404 The complementary plasmids were derived from pRY107 (Kan resistance) vector. The full *lon*
405 gene, including the coding region and ~500 bp upstream of the start codon, was PCR-amplified
406 using primers OLU228/OLU229. The PCR products were ligated with EcoRI/XbaI-digested
407 pRY107 using the NEBuilder® HiFi DNA Assembly Cloning Kit. The complementary plasmid
408 pRY107-*lon* was transformed into *C. jejuni Δlon* strain and the complementary transformants
409 were selected on the MHAKan20 agar. To construct the complementary plasmid of *clpP*, the full
410 *clpP* gene, including the coding region and ~400 bp upstream of the start codon, was PCR-
411 amplified using the primers OLU230/231 and cloned into pRY107 subsequently. The
412 complementary plasmid pRY107-*clpP* was transformed into *C. jejuni ΔclpP* strain and the
413 complementary transformants were selected on the MHAKan20 agar.
414
415 The *spoT* mutant of *C. jejuni* was generated using the similar technique above. Briefly, upstream
416 and downstream regions flanking *spoT* (*spoT*^{up}, *spoT*^{down}) were PCR-amplified using the primer
417 pairs *spoT*-FF/*spoT*-FR and *sopT*-RF/*sopT*-RR, respectively. The Kan^R gene was amplified from
418 pUC18K2 using the primer pair *kan*-F/*kan*-R. The engineered plasmid pUC19-*spoT*^{up}-*Kan*^{R}-
419 *spoT*^{down} was transformed into *C. jejuni* strain F38011, followed by selection on *kan* (50 µg/mL)
420 agar, subsequently. Deletion of *spoT* was confirmed by PCR.
421
422 The *recA* deletion mutant of *C. jejuni* was generated using a similar protocol as described above.
423 Briefly, upstream and downstream regions flanking *recA* (*recA*^{up}, *recA*^{down}) were PCR-amplified
424 using the primer pairs *recA*-FF/*recA*-FR and *recA*-RF/*recA*-RR, respectively. The Cm^R gene was
425 amplified from pRY111 using the primer pair *cm*-F/*cm*-R. The engineered plasmid pUC19-

426 *recA*^{up}-Cm^{R}- *recA*^{down} was transformed into *C. jejuni* strain F38011, followed by selection on the
427 MHAkan50 agar subsequently. Deletion of *recA* was confirmed by PCR.
428
429 **Antibiotic killing and isolation of persister cells**
430 Overnight *C. jejuni* culture was diluted to ~log 8 CFU/mL in MHB containing either ampicillin
431 (100 µg/mL) or ciprofloxacin (1 µg/mL). The bacterial culture was kept with shaking at 37°C in
432 a microaerobic condition. At indicated time points, aliquots were collected, centrifuged, washed
433 with PBS, and plated on MHA. After incubation for 24 hr, 10-100 colonies were enumerated for
434 each data point unless further noted. Along with antibiotic exposure, development of a biphasic
435 killing curve could confirm the formation of *C. jejuni* persister cells.
436
437 **Determination of antibiotic MIC**
438 MIC was determined using the broth microdilution method. Overnight bacterial culture was
439 diluted to ~log7 CFU/mL in MHB and added into 96-well flat-bottom clear polypropylene plates
440 (Corning) with two-fold dilutions of antibiotic in a total volume of 100 µL. Plates were incubated
441 at 37°C for 24 hr and then the absorbance at OD_{600} was measured using a Spectramax M3
442 microplate reader.
443
444 **Lipid peroxidation**
445 Lipid peroxidation in *C. jejuni* cells was determined using the BODIPY™581/591 C11 sensor kit
446 (Invitrogen™) according to the manufacturer's instructions. Briefly, overnight cultures of wild-
447 type *C. jejuni* F38011 and mutant strains were stained with dye in the dark for 1 hr and then
448 added to 96-well black microplates (~log 8 cells per well). Cells were treated with hydrogen
449 peroxide (100 µM), ampicillin (100 µg/mL), or ciprofloxacin (1 µg/mL) for 2 hr. Lipid
450 peroxidation level was evaluated as the relative increase in fluorescence emission at 525 nm.
451
452 **RNA-seq analysis**
453 Total RNA of both untreated *C. jejuni* cells and persister cells was extracted using the RNeasy
454 Mini Kit (Qiagen). Ribosomal RNA was removed by the RiboMinus Transcriptome Isolation Kit
455 (Invitrogen) and mRNA was then purified using the RNeasy Mini Spin columns (Qiagen). The
456 resulting transcriptome RNA was used for the construction of RNA-seq library using NEB Next
457 mRNA Library Prep Reagent set from Illumina (NEB) according to the manufacturer's protocol.
458 These constructed libraries were sequenced by Illumina HiSeq 2000 platform by paired-end
459 chemistry. Sequence reads processing, mapping to *C. jejuni* NCTC 11168 genome (NC_002163),
460 and quantification of differential expression (RPKM) were conducted using CLC genomic
461 workbench. The functional annotation of genes was conducted in the Kyoto Encyclopedia of
462 Genes and Genomes (KEGG) database. Statistical significance is referred to as absolute log 2-
463 fold change >1 and *p*-value <0.5.
464

465 **Quantitative PCR analysis**
466 *C. jejuni* cells from both untreated cultures and cultures exposed to antibiotics for 4 hr were
467 collected for RNA extraction using the RNeasy mini kit (Qiagen). Total RNA concentration and
468 purity were determined using a Nanodrop 2000 Spectrophotometer (Thermo Scientific). The
469 cDNA was produced via SuperScript™ II Reverse Transcriptase (Invitrogen). qPCR was
470 performed using cDNA from bacterial samples with Power SYBR green PCR Master Mix
471 (Applied Biosystems, Warrington, United Kingdom) on an ABI Prism 7000 Fast instrument (Life
472 Technologies). The primers used for qPCR validation are listed in **Table S1**. Housekeeping genes
473 *gyrA* and *rpoA* in *Campylobacter* were used as the internal controls. A total of 7 genes that were
474 detected as differentially expressed in the RNA-seq results were selected for validation.
475
476 **Label-free quantitative proteomics by LC-MS/MS**
477 *C. jejuni* persister cells were collected and cell pellets were suspended in ammonium bicarbonate
478 (100 mM) and lysed by bead beating on ice. The lysates were diluted and digested with trypsin.
479 Digested peptides were desalted, and their concentration was determined by the bicinchoninic
480 acid protein assay. The sample was then analyzed by LC-MS/MS using a Waters
481 nanoACQUITY UPLC® system (Milford, United States) coupled with a Q Exactive HF hybrid
482 quadrupole-Orbitrap mass spectrometer (Thermo Scientific, San Jose, United States). Raw mass
483 spectrometry data were processed using the MaxQuant proteomics platform [88]. The false
484 discovery rate was set at 0.01 at the peptide and protein levels. Proteins were identified with at
485 least 2 peptides of a minimum length of 6 amino acids in Uniprot database using *C. jejuni* NTCT
486 11168 proteome (UP000031762). Protein relative abundance was quantified using the
487 MaxQuant-LFQ algorithm [89]. The sample with a measured LFQ intensity in at least two out of
488 the three samples was subjected to quantification. Statistical significance is referred to as an
489 absolute log 2-fold change>1 and a *p*-value for a two-tailed t-test <0.05.
490
491 **COG category annotation**
492 PSI-BLAST (version 2.2.31+) was used to categorize proteins of *C. jejuni* F38011 according to
493 the COG database with a default cut-off value [89]. Top PSI-BLAST hits were manually curated.
494
495 **Metabolomics and lipidomics**
496 Both untreated and persister cells were subjected to dual extraction for both hydrophilic
497 metabolomics and hydrophobic lipidomics. Briefly, 10 μL of ^{13}C labeled hydrophilic metabolites
498 and 10 μL of odd-chain lipid molecules were added to bacterial samples as the internal standards.
499 Then, 270 μL of ice-cold methanol (kept at -20°C) was added to quench cell metabolism. The
500 metabolites were released by three freeze-thaw cycles, including flash freezing in liquid nitrogen
501 for 1 min and sonication in ice water for 15 min. After adding 900 μL of methyl tert-butyl ether
502 (MTBE), the samples were sonicated in ice water for 30 min to extract hydrophobic molecules.
503 Next, the samples were mixed with 315 μL of cold H_2O and centrifuged at 20,817 ×*g* and 10°C
504 for 2 min to achieve a clear phase separation between the hydrophilic methanol-H_2O layer

505 (bottom) and the hydrophobic MTBE layer (top). The MTBE layer was collected, speed vacuum
506 dried, reconstituted with 100 μL of isopropanol alcohol/acetonitrile (1:1, v/v), and stored at -
507 80°C for further lipidomic analysis. The methanol-H_2O layer of the samples was kept at -20°C
508 for 2 hr to precipitate the proteins. After centrifugation at 20,817 ×*g* and 4°C for 15 min, the
509 supernatant was collected. This aqueous solution was dried in a speed-vacuum drier,
510 reconstituted using 100 μL of acetonitrile/H_2O (1:1, v/v), and stored at -80°C for further
511 metabolomic analysis. Quality control samples for both metabolomics and lipidomics were
512 prepared by mixing 10 μL of each sample. One method-blank sample (*i.e.*, an empty tube
513 subjected to the overall extraction procedure) and two solvent-blank samples (*i.e.*, reconstitution
514 solvent) were prepared as the negative controls.
515
516 Metabolomic (positive and negative) and lipidomic (negative) analyses of the samples were
517 conducted using an Agilent 1290 infinite UHPLC system (Agilent Technologies, Palo Alto, CA)
518 coupled with a Bruker Impact II quadrupole-time-of-flight (QTOF) mass spectrometer (Bruker
519 Daltonics, Bremen, Germany). For hydrophilic metabolomic analysis, samples were separated on
520 a SeQuant ZIC-pHILIC column (2.1 × 150 mm, 3.5 μm, 100 Å). Mobile phase A contained 5
521 mM NH_4Ac in 95% H_2O and 5% acetonitrile and mobile phase B constituted of 5 mM NH_4Ac in
522 5% H_2O and 95% acetonitrile. The pH of mobile phase A was adjusted to 5 for positive mass
523 spectral collection, and the pH was maintained at 9.8 for negative mass spectral collection.
524 Sample elution was achieved using a linear gradient at 30°C with a flow rate of 200 μL/min.
525 Specifically, the gradient started with 95% B for the first 3 min, decreased to 75% B over 4 min,
526 then to 25% B at 12 min, again to 5% B at 14 min, and finally maintained at 5% for 4 min. The
527 column was then equilibrated at 95% B for 18 min before the injection of the next sample.
528 Sample injection volume was optimized using a quality control sample to maximize spectral
529 intensity and avoid signal saturation.
530
531 For lipidomic negative analysis, samples were separated on a Waters Acquity UPLC BEH C_{18}
532 column (1 × 100 mm, 1.7 μm, 130 Å). The mobile phases for the separation were A: 5 mM
533 ammonium formate in acetonitrile/H_2O (6:4 v/v) and B: 5 mM ammonium formate in
534 isopropanol alcohol/acetonitrile (9:1, v/v). The gradient sample elution program started with 5%
535 B, increased to 40% B at 8 min, again to 70% B at 14 min, finally reached 95% B at 20 min, and
536 maintained for 3 min. The column was then equilibrated at 5% B for 9 min before the next
537 injection. The column was maintained at 25°C with a flow rate of 150 μL/min. Sample injection
538 volume was optimized using the same approach as that for metabolomic analysis. An
539 electrospray ionization source was used to ionize metabolites for MS detection and spectral
540 information was recorded using the data-dependent MS/MS approach (auto MS/MS). The
541 spectra for auto MS/MS were collected using a spectral rate of 8 Hz and *m/z* range of 50 to
542 1,200. For the auto MS/MS method, the MS/MS spectra were acquired using a stepping collision
543 energy of 40 eV to 120 eV, an intensity threshold of 300, a cycle time of 3 s, a smart exclusion
544 after two spectra, and a precursor reconsideration for intensity difference >1.8. The data-

545 dependent LC-MS/MS results were normalized to total protein content according to the Bradford
546 assay and processed using MS-DIAL (RIKEN, version 3.52). All the metabolic features with
547 MS/MS spectra were manually confirmed using the MS-Finder (RIKEN, version 3.20), METLIN
548 (Scripps Research), or an in-house metabolic library with an m/z tolerance of 5 ppm.
549 Significantly regulated metabolic features were defined as absolute log 2-fold >2 and *p*-value for
550 two-tailed t-test <0.05.
551
552 **Gene set enrichment analysis**
553 Gene set enrichment analysis (GSEA) was conducted using the Java (GSEA 3.0)-based graphical
554 user interface with a pre-ranked list of the classic enrichment statistics [90, 91]. GSEA was used
555 to determine whether a pre-defined set of genes/proteins is significantly different between
556 persister cells and untreated cells. The entire list of genes/proteins was ranked according to the
557 expression difference between persister cells and untreated cells. The cumulative distribution
558 function was constructed by performing 1000 random gene set membership assignments.
559
560 **Visualization of the enrichment map**
561 The significantly enriched terms in transcriptome and proteome analysis were visualized in
562 Cytoscape 3.7.1 [92]. Enrichment maps were built with stringent pathway similarity scores
563 (Jaccard and overlap combined coefficient 0.6) and manually curated for the most representative
564 groups of similar pathways and biological processes.
565
566 **Seahorse extracellular flux analysis**
567 Extracellular flux analysis was performed using an XFe96 Extracellular Flux Analyzer to
568 measure bacterial respiration as oxygen consumption rate (OCR). This assay was adapted from a
569 previously published method with modifications [34]. Overnight cultures of *C. jejuni* F38011
570 wild-type and the *ΔclpP* were grown in MHB at 37°C with shaking at 175 rpm in a CO_2
571 incubator shaker supplied with 10% CO_2. Cultures were grown to an OD_{600} of ~0.3 and then
572 diluted in fresh MHB to an OD_{600} of 0.06, corresponding to ~2×10^8 CFU/mL. For plate
573 preparation, XF cell culture microplates were coated with poly-D-lysine (PDL). Briefly, 15 µL of
574 1 mg/mL PDL prepared in 100 mM Tris-HCl (pH 8.4) was added to each well, followed by
575 overnight drying in a biosafety cabinet and two rinses with distilled water. Then, 90 µL of
576 diluted bacterial suspension was added to each well. Cells were attached to the PDL-coated wells
577 by centrifugation at 3,313 x *g* for 10 min in a benchtop swinging-bucket centrifuge to generate a
578 monolayer of adhered cells. After centrifugation, 90 µL of MHB was gently added to each well
579 to bring the final pre-injection volume to 180 µL. Following calibration with equilibration
580 enabled, basal OCR was recorded before antibiotic addition to confirm uniform cell seeding. The
581 baseline phase consisted of 3 measurement cycles, each including 1.5 min of mixing, 1.5 min of
582 waiting, and 3 min of measurement for a total baseline duration of 18 min. For treatment
583 conditions, 20 µL of 10× antibiotic stock was injected through port A to achieve final
584 concentrations of 20 µg/mL ampicillin or 0.2 µg/mL ciprofloxacin. For untreated controls, 20 µL
585 of MHB alone was injected. OCR was then monitored using 30 measurement cycles, each

586 consisting of 1.5 min of mixing, 1.5 min of waiting, and 3 min of measurement for a total post-
587 injection duration of 3 hr. Wells receiving MHB alone served as no-treatment controls.
588
589 OCR values were normalized to the number of viable cells, expressed as CFU/mL, determined
590 by plating assay. For normalization, bacteria were cultured and treated in parallel on an XF Cell
591 Culture Microplate under the same conditions as those used for the Seahorse assay. At 30 min
592 after the aerobic incubation, aliquots were collected from parallel wells, serially diluted in sterile
593 PBS, and plated onto MHA for colony enumeration. After incubation under microaerophilic
594 conditions at 37°C for 48 hours, colonies were counted and viable cell numbers were calculated
595 as CFU/mL. OCR values were then normalized to the corresponding viable cell counts obtained
596 from matched treatment groups.
597
598 **Protein extraction and Western blot analysis**
599 *C. jejuni* cells grown in MHB were harvested by centrifugation, and total protein was extracted
600 using B-PER II bacterial protein extraction reagent supplemented with EDTA-free protease
601 inhibitor, lysozyme, and DNase I according to the manufacturer's instructions. Protein samples
602 were prepared in LDS sample buffer supplemented with reducing agent and separated on 4-12%
603 Bis-Tris gels in MES SDS running buffer with antioxidant added to the inner chamber at 120 V
604 for 100 min. Proteins were then transferred onto 0.45-µm PVDF membranes. Before transfer,
605 membranes were activated in methanol for 1 min, and gels were equilibrated in Towbin transfer
606 buffer without SDS or methanol for 10 min. Transfer was performed using a Trans-Blot Turbo
607 Transfer System in Towbin transfer buffer without SDS and methanol. Membranes were blocked
608 in 5% bovine serum albumin in PBST for 1 hr at room temperature and incubated overnight at
609 4°C with anti-CydA antibody diluted 1:5,000 in 5% bovine serum albumin in PBST. After three
610 washes with PBST for 10 min each, membranes were incubated for 1 hr at room temperature
611 with HRP-conjugated goat anti-rabbit secondary antibody diluted 1:5,000 in 5% bovine serum
612 albumin in PBST, followed by five washes with PBST for 10 min each. Protein bands were
613 detected using enhanced chemiluminescence substrate. Membranes were incubated with
614 substrate for 1 min in the dark and imaged by chemiluminescence. Ponceau S and
615 chemiluminescence images were merged for figure preparation.
616
617 **RAW 264.7 macrophage infection assay**
618 RAW 264.7 murine macrophages were maintained in Dulbecco's modified Eagle medium
619 supplemented with 10% fetal bovine serum at 37°C in a humidified incubator with 5% CO_2 as
620 previously described with modifications. For infection assays, cells were seeded in 24-well plates
621 and infected with *C. jejuni* F38011 wild-type or the *ΔclpP* mutant at a multiplicity of infection
622 (MOI) of 100 [93]. Following infection, macrophages were incubated for 3 hr to assess bacterial
623 adherence. At the indicated time points, monolayers were washed twice with PBS to remove
624 non-adherent bacteria. For adherence assays, macrophages were lysed with 0.1% Triton X-100,
625 and recovered bacteria were serially diluted and plated for CFU enumeration. To assess bacterial
626 survival in the host-associated environment, infected macrophages were further incubated until

627 the indicated time points, lysed, and viable bacteria were quantified by the plating assay.
628 Bacterial counts were expressed as CFU per well and compared between strains.
629
630 **Mouse colonization assay**
631 To determine the contribution of ClpP to host colonization, 8-week-old Sigirr^-/- mice were
632 orally inoculated with *C. jejuni* 81-176, F38011 wild-type or the *Δlon* and *ΔclpP* mutants at a
633 dose of ~1×10^7 CFU per mouse, following an established protocol [52]. At the indicated
634 timepoints post-infection, mice were euthanized, and intestinal tissues and/or intestinal contents
635 were collected. Samples were suspended in sterile PBS, homogenized, serially diluted, and
636 plated on MHA containing selective supplements. Plates were incubated for 48 hr at 42°C under
637 microaerobic conditions, after which colonies were enumerated. Bacterial burdens were
638 calculated and expressed as CFU per gram of tissue or intestinal content. Animal experiments
639 were conducted under protocol A11-290, approved by the University of British Columbia
640 Animal Care Committee, in accordance with Canadian Council of Animal Care (CCAC)
641 guidelines. Mice were monitored throughout infection and were euthanized upon signs of severe
642 distress or body weight loss exceeding 15%.
643
644 **Histology, pathological scoring and immunofluorescent staining**
645 Histological analysis was conducted according to an established protocol with minor
646 modifications [52]. Intestinal tissues were collected from infected mice, fixed in 10% neutral-
647 buffered formalin, paraffin embedded, and sectioned. For histological evaluation, tissue sections
648 were stained using hematoxylin and eosin and examined microscopically for the presence and
649 localization of *C. jejuni* at the intestinal surface.
650

ACKNOWLEDGEMENTS

This work was supported by funds provided to X.L. from Natural Sciences and Engineering Research Council of Canada (NSERC RGPIN-2019-03960, RGPIN-2019-00024, RGPIN-2025-03996), Canada Research Chairs Program (CRC-2024-00011), Sector Innovation Program of Genome Canada and Genome British Columbia, Genomics Integration Program of Genome Québec, Fonds de recherche du Québec – Nature et technologies, and Canadian Poultry Research Council.

FIGURES

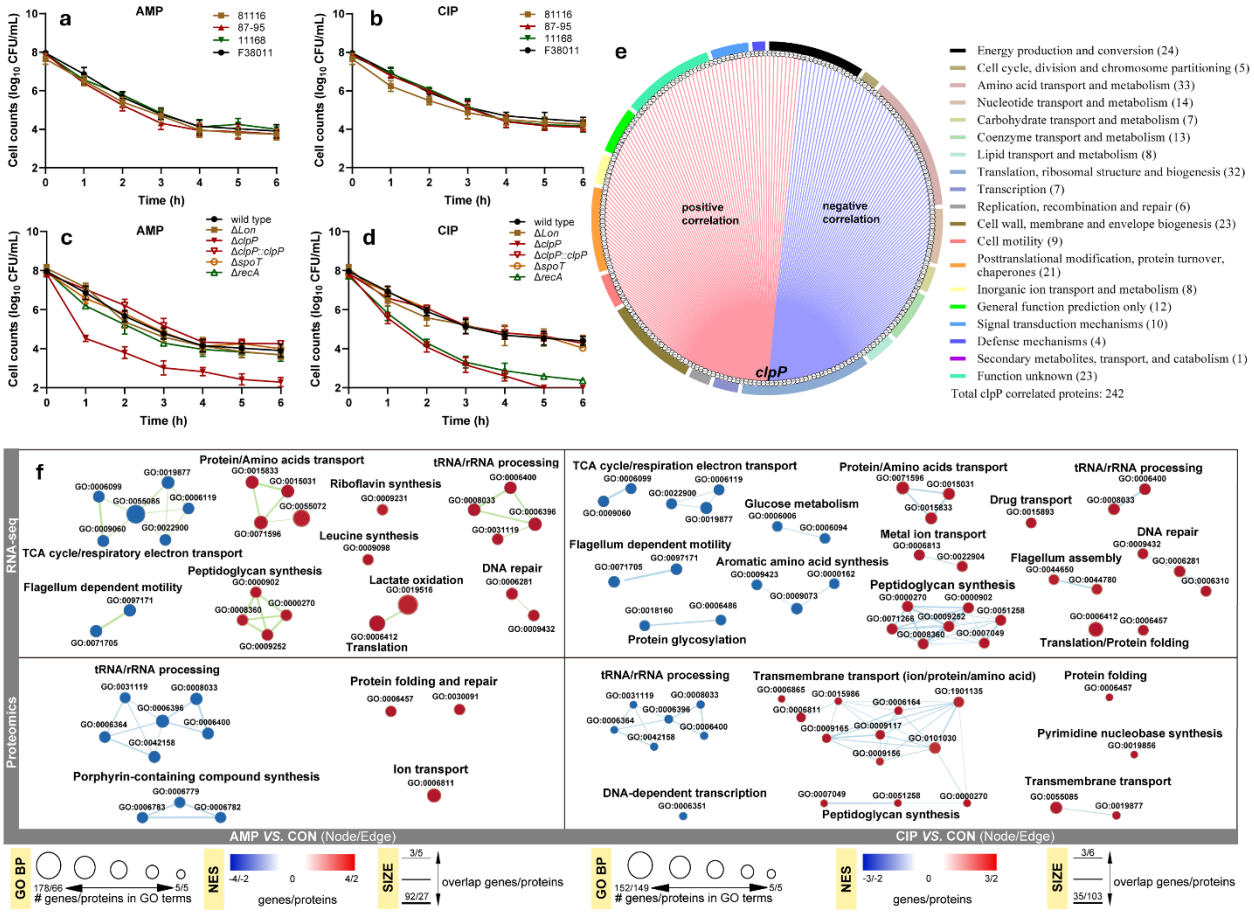

Figure 1. *clpP* is critical for *Campylobacter jejuni* persisters to tolerate ampicillin (AMP) and ciprofloxacin (CIP). (a, b) Time-killing curves of AMP (a) and CIP (b) against four *C. jejuni* strains: 81116 (dark yellow squares), 87-95 (red triangles), 11168 (green inverted triangles), and F38011 (black circles). Cultures were grown to an optical density of 0.3 and then diluted to approximately log 8 CFU/mL in Mueller–Hinton (MH) broth containing either ampicillin (100 µg/mL) or ciprofloxacin (1 µg/mL). **(c, d)** Time-killing curves of AMP (c) and CIP (d) against wild-type F38011 (black circles), the *Δlon* mutant (dark yellow squares), *ΔclpP* mutant (red inverted triangles), *ΔspoT* mutant (orange open circles), *ΔrecA* mutant (green open triangles), and the *clpP*-complemented strain (*ΔclpP::clpP*; red open inverted triangles). **(e)** Cluster of Orthologous Groups (COG) classification of proteins strongly correlated with *clpP*. A total of 241proteins were identified based on an absolute Pearson correlation coefficient >0.8 and $p < 0.05$. COG analysis grouped these *clpP*-correlated proteins into 19 functional categories; the number of proteins assigned to each category is indicated in parentheses. **(f)** Gene set enrichment analysis (GSEA) of transcriptomic and proteomic profiles of *C. jejuni* persisters. GSEA was performed using pre-ranked lists of all genes or proteins based on differential expression between antibiotic-selected persister cells and untreated cells. The cumulative distribution function was generated using 1,000 random gene set membership permutations. Significantly enriched terms from transcriptomic and proteomic analyses were visualized in Cytoscape 3.7.1. GO enrichments were constructed using a stringent pathway similarity threshold (combined Jaccard and overlap

681 coefficient = 0.6) and manually curated to highlight representative biological process (GO BP).
682 Node size corresponds to gene set size, and node color indicates enrichment in antibiotic-selected
683 persister cells (red; upregulated after antibiotic treatment) or untreated cells (blue; downregulated
684 after antibiotic treatment). Edge thickness represents the degree of gene overlap between
685 connected gene sets. Data are presented as mean ± SD from at least three independently grown
686 cultures.

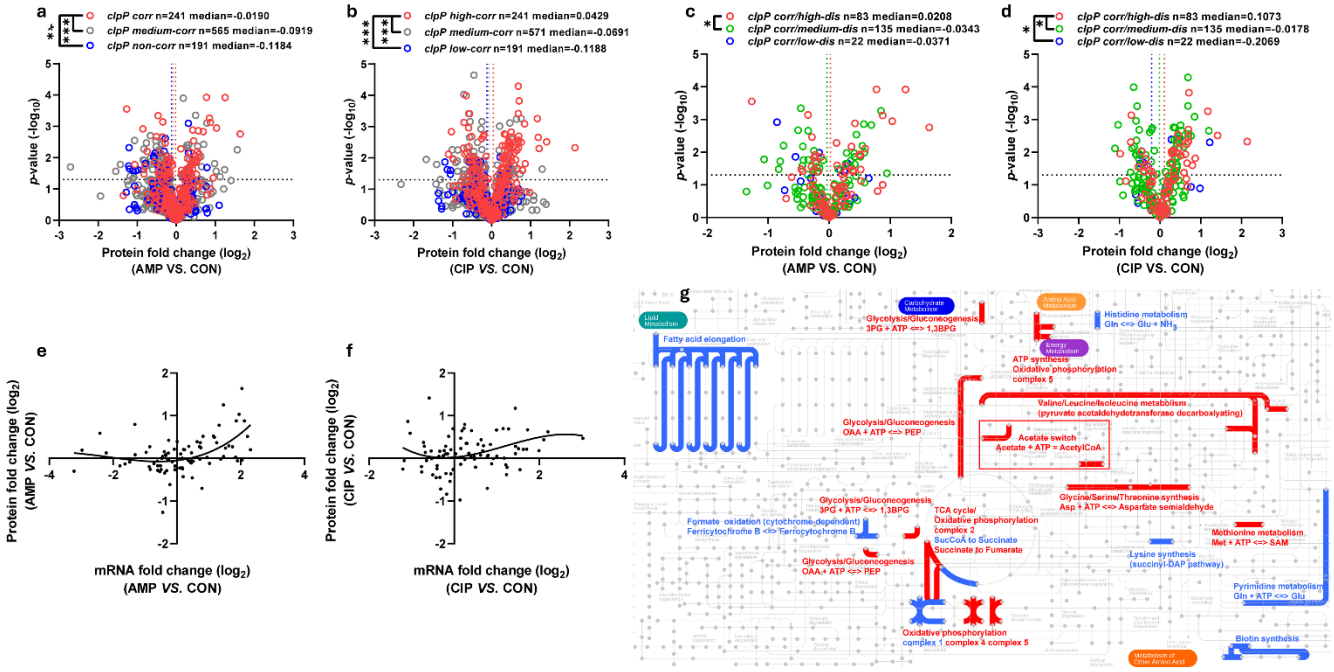

Figure 2. *clpP*-associated high-disorder proteins define metabolically active functions in *C. jejuni* persisters. (a, b) Distribution of protein fold changes in *C. jejuni* F38011 persisters after ampicillin (a) or ciprofloxacin (b) treatment, stratified by the correlation between protein abundance and *clpP* expression. Pearson correlation analysis was used to determine abundance correlation with *clpP*. *clpP*-correlated features were defined as proteins with an absolute correlation coefficient $|r| > 0.8$ and $p < 0.05$, whereas non-correlated features were defined as proteins with $|r| < 0.2$and $p < 0.05$. **(c, d)** Distribution of protein fold changes among *clpP*-correlated proteins was further stratified by predicted disorder tendency after ampicillin (c) or ciprofloxacin (d) treatment. Disorder tendency was predicted using DFLpred based on the proportion of disordered flexible linker residues within each protein sequence. High disorder proteins were determined as disordered flexible linker residues accounting for >30% of the total sequences. Non-disorder proteins were determined as disordered flexible linker residues accounting for <10% of the total sequences. Among the *clpP*-correlated proteins detected in both conditions, 83 were classified as high-disorder, 135 as medium-disorder, and 22 as low-disorder. **(e, f)** Relationship between mRNA and protein log2 fold changes for *clpP*-correlated/high-disorder features in persisters after ampicillin (e) or ciprofloxacin (f) treatment. Differentially expressed genes and proteins were compared across the corresponding pairwise contrasts. **(g)** Global metabolic map derived from *clpP*-correlated/high-disorder features. Red indicates promoted activity, whereas blue indicates inhibited activity.

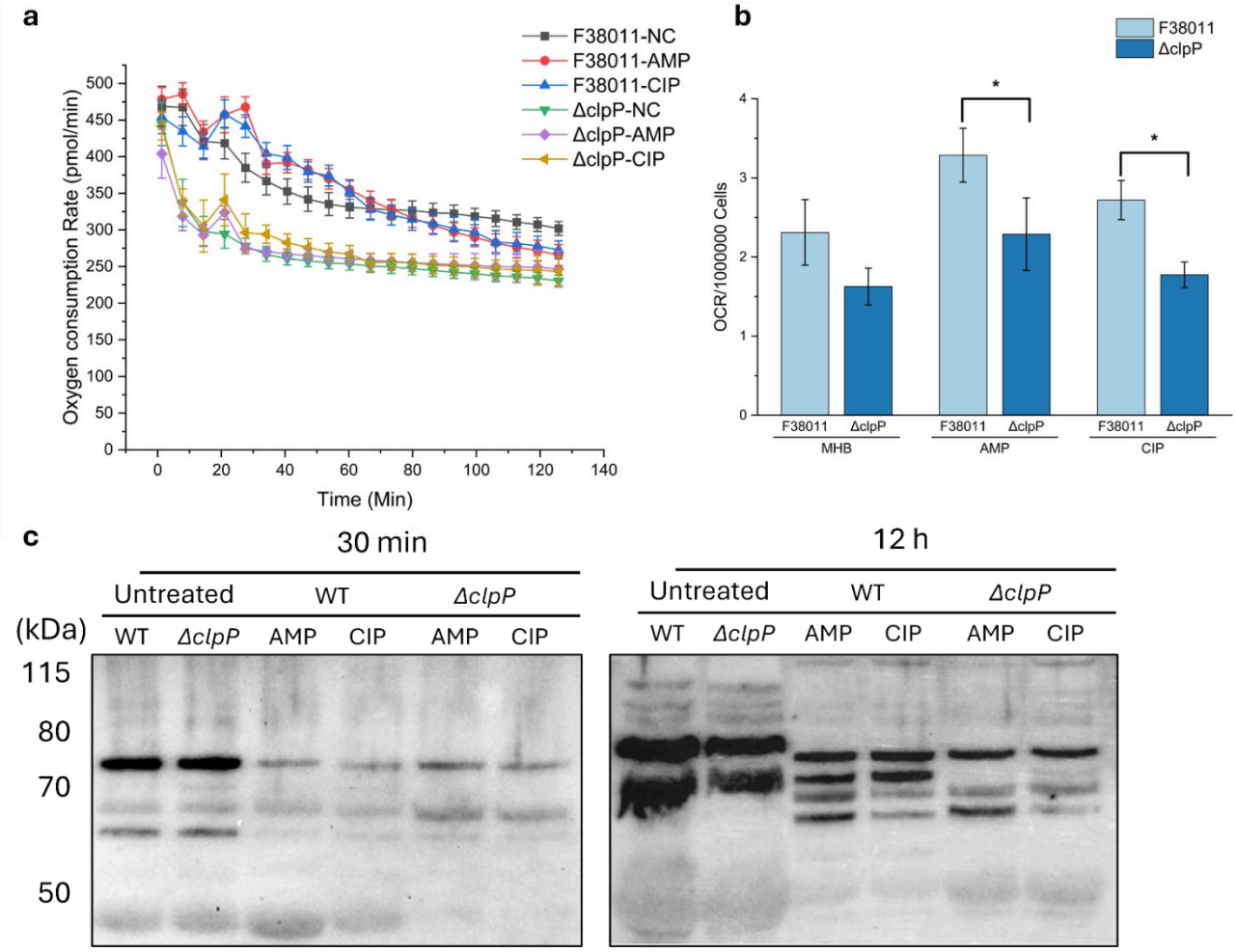

Figure 3. ClpP supports the antibiotic-induced respiratory response and bd-like terminal oxidase integrity in *C. jejuni*. (a) Real-time changes in oxygen consumption rate (OCR; pmol O_2/min) in wild-type F38011 and the *ΔclpP* mutant in response to antibiotic treatment were measured using a Seahorse XFe Extracellular Flux Analyzer. OCR was monitored over time in untreated control cells (NC) and in cells exposed to ampicillin (AMP) or ciprofloxacin (CIP) at 20 µg/mL and 0.2 µg/mL, respectively. Antibiotic treatment induced a transient increase in respiration, and the wild-type strain displayed a stronger and more sustained OCR response than the *ΔclpP* mutant. Data represent mean ± SD of 12 technical replicates. **(b)** Normalized OCR per live cell. (*$p < 0.05$). **(c)** Western blot analysis of the bd-like terminal oxidase subunit CydA in wild-type F38011 and *ΔclpP* cells exposed to ampicillin or ciprofloxacin at 10 µg/mL and 0.1 µg/mL for 30 min or 12 h. Untreated cells served as no-antibiotic controls. Lane order in each panel is: untreated WT, untreated *ΔclpP*, WT + AMP, WT + CIP, *ΔclpP* + AMP, and *ΔclpP* + CIP. At 30 min, CydA-associated signals were weak across antibiotic-treated samples. By 12 h, wild-type cells retained a clearer multi-band CydA pattern, whereas *ΔclpP* cells showed an altered banding pattern characterized by reduction of the lower CydA-associated bands despite retention of the upper band. Molecular mass markers (kDa) are indicated on the left.

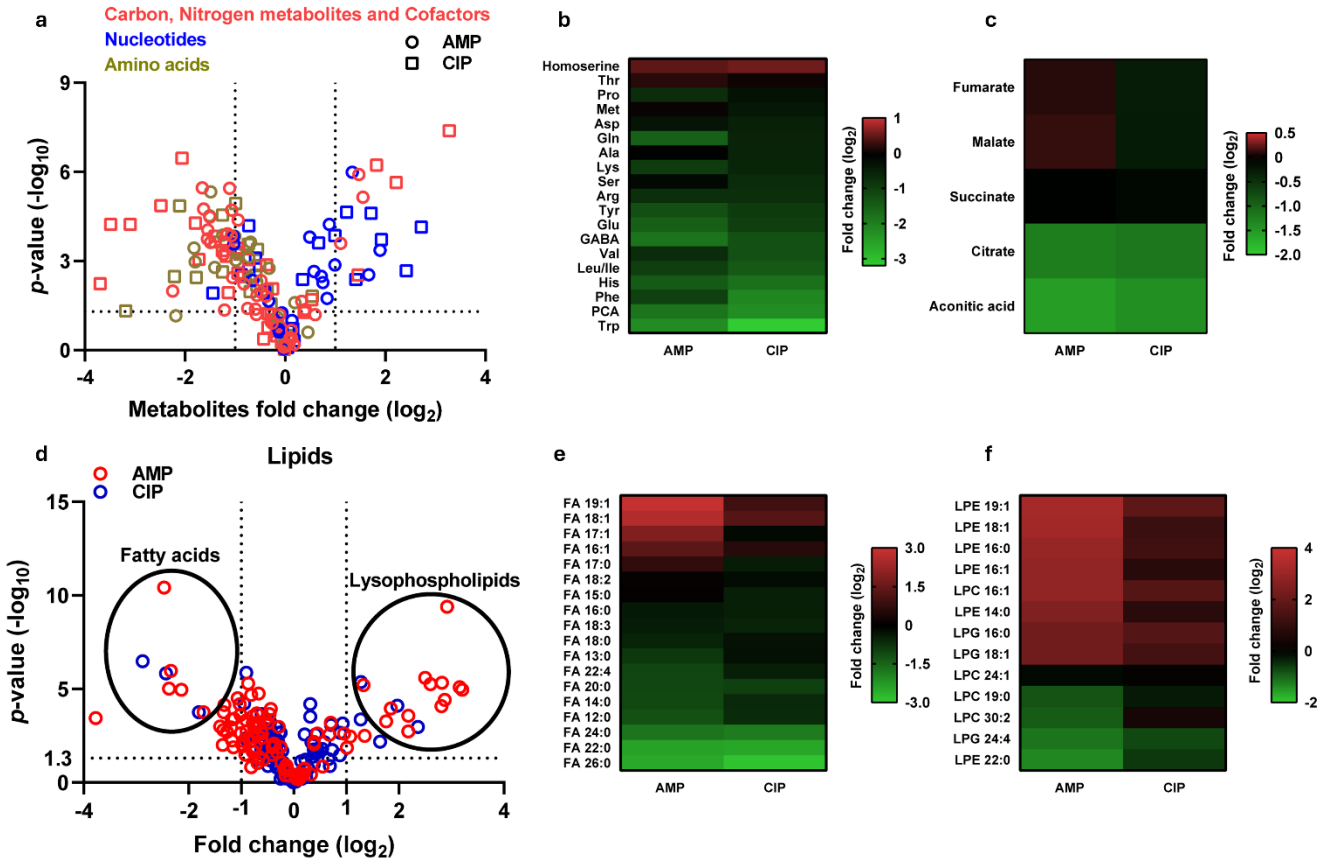

Figure 4. *C. jejuni* F38011 persisters exhibited distinct metabolomic and lipidomic features compared with untreated growing cells. (a) Volcano plot showing changes in relative metabolite abundance in persister cells selected by AMP or CIP compared with untreated cells. Metabolites are color-coded by functional class, including carbon, nitrogen, and cofactor-related metabolites, nucleotides, and amino acids. **(b)** Heatmap showing relative abundance changes of selected amino acids in AMP and CIP selected persister cells. **(c)** Heatmap showing relative abundance changes of selected TCA cycle intermediates in AMP and CIP selected persister cells. **(d)** Volcano plot showing changes in relative lipid abundance in persister cells selected by AMP or CIP compared with untreated cells. Fatty acids and lysophospholipids are highlighted. **(e)** Heatmap showing relative abundance changes of fatty acids in *C. jejuni* persister cells. **(f)** Heatmap showing relative abundance changes of lysophospholipids in *C. jejuni* persister cells.

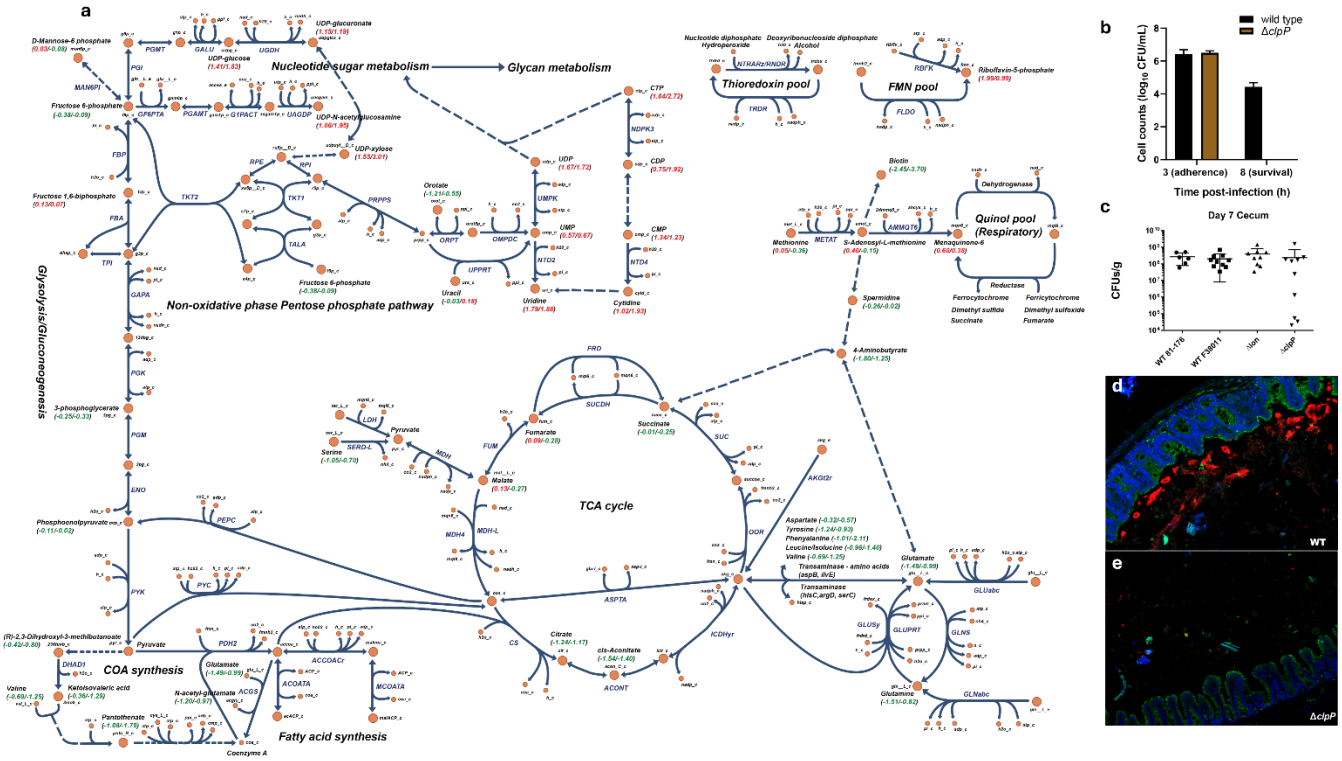

Figure 5. Metabolic reprogramming of *C. jejuni* persisters and reduced host-associated survival of the *clpP* mutant. (a) Core metabolic map illustrating metabolic reprogramming in *C. jejuni* persister cells relative to untreated growing cells. Relative metabolite abundance changes are annotated on the network, with red values indicating increased abundance (log2 fold change) and green values indicating decreased abundance (log fold change). Left: AMP; Right: CIP. **(b)** Survival of wild-type F38011 and the persistence-compromised *clpP* mutant in macrophages. **(c)** Cecal colonization levels of wild-type F38011 and the *clpP* mutant in *sigirr*^-/- mice. **(d, e)** Representative images showing localization of wild-type F38011 (d) and the *clpP* mutant (e) in the cecum of *sigirr*^-/- mice.

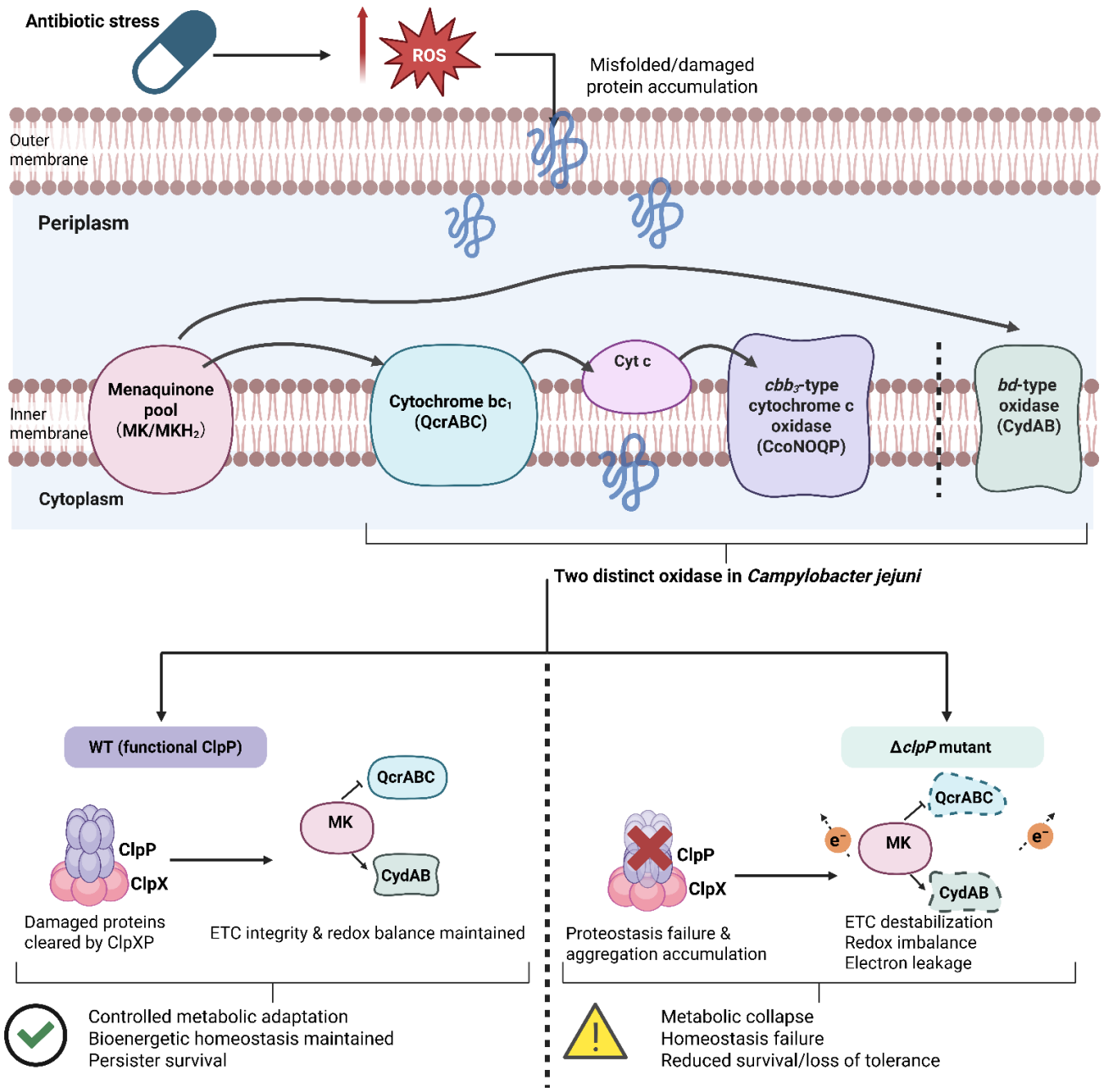

Figure 6. Proposed model of ClpP-dependent proteostasis and respiratory/redox homeostasis during antibiotic tolerance in *C. jejuni*. Under optimal microaerobic growth conditions, *C. jejuni* maintains efficient respiratory activity and energy conservation while ClpP-dependent proteostasis preserves protein integrity and supports overall cellular homeostasis. Upon exposure to bactericidal antibiotics and associated oxidative stress, cells enter a stress-adaptive tolerant state characterized by controlled metabolic downshift, respiratory remodeling, redox-oriented metabolic adaptation, and increased reliance on protein quality control. In this state, ClpP-mediated clearance of damaged or misfolded proteins is proposed to preserve respiratory chain integrity, maintain terminal oxidase function, and sustain survival-supportive homeostasis (**Bottom Left**). In the absence of ClpP, damaged proteins accumulate and

760 proteostasis becomes disrupted, leading to impaired respiratory adaptation, amplified redox
761 imbalance, membrane-associated damage, and reduced survival capacity under both antibiotic-
762 treated and host-associated conditions (**Bottom Right**). This model summarizes the major
763 conclusions derived from the multi-omics, respiratory, oxidative stress, macrophage infection,
764 and mouse colonization analyses in this study.

765

766 **EXTENDED DATA**

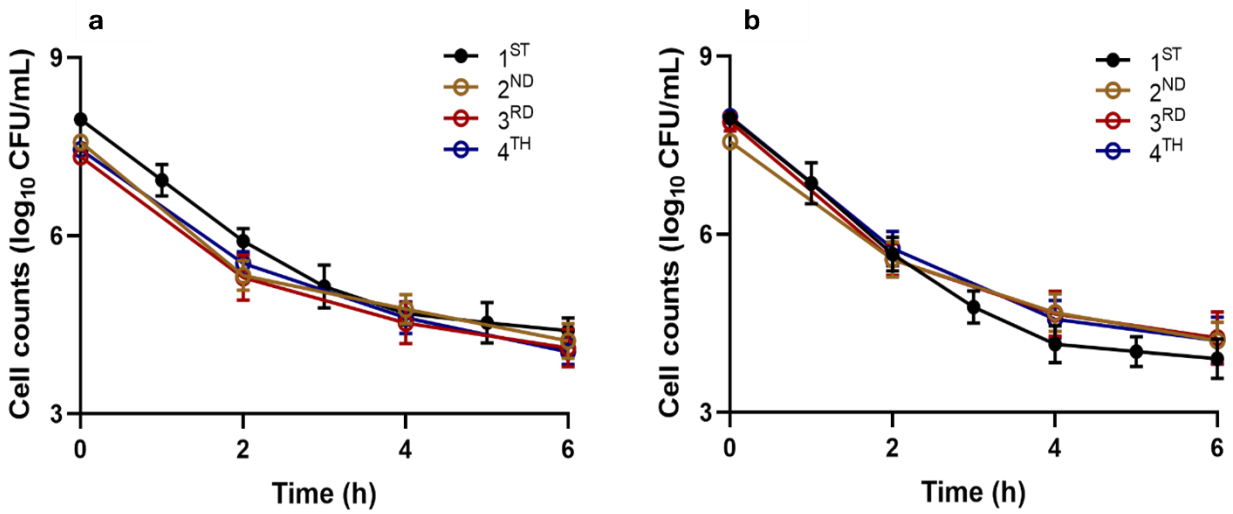

767

768 **Extended Data Figure 1. *C. jejuni* F38011 wild type strain were subjected to multiple**
769 **rounds of challenges with ampicillin (a) and ciprofloxacin (b) for multiple rounds, and no**
770 **detectable resistance observed.**

771

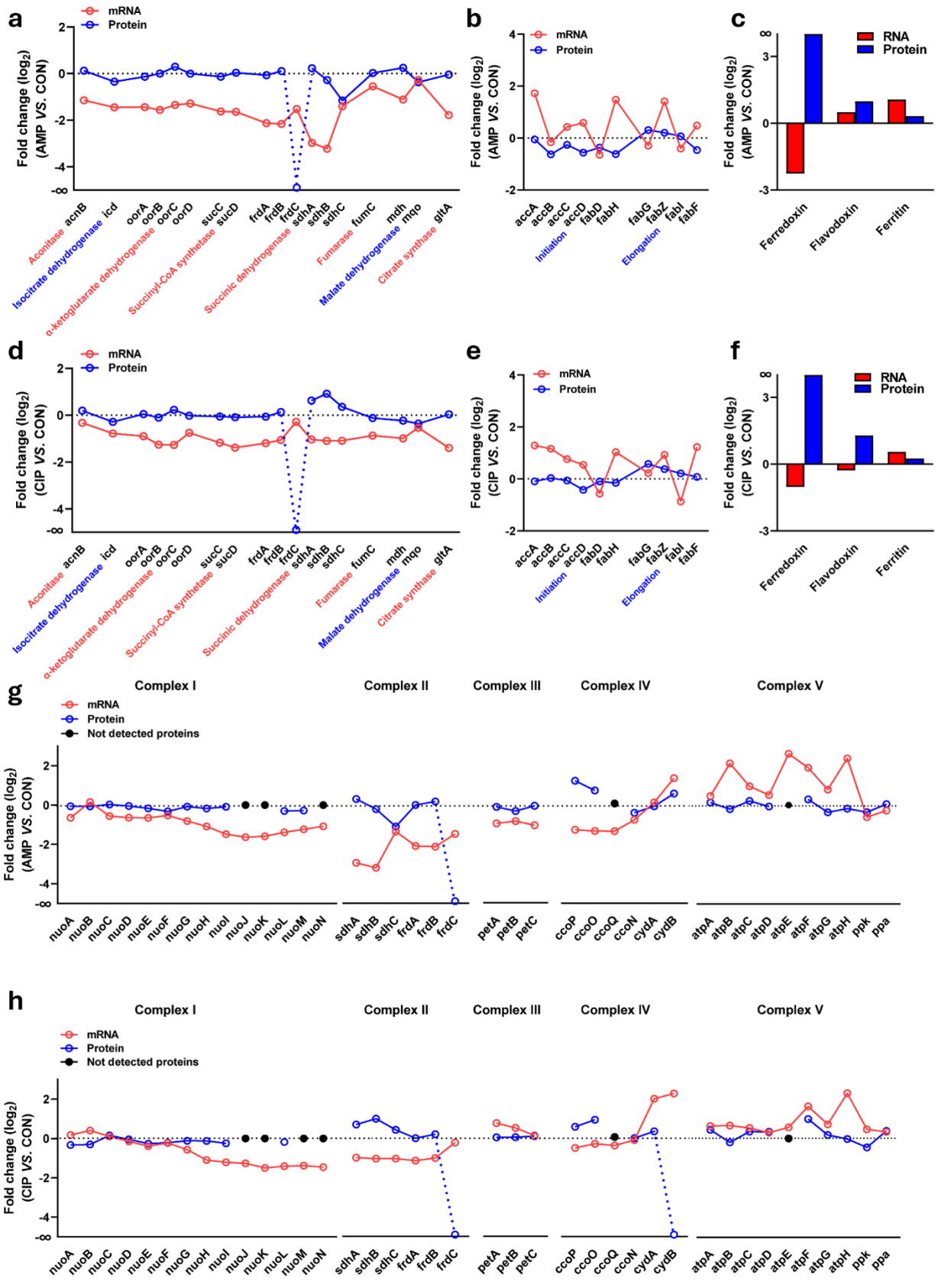
a
mRNA
Protein
Fold change (log2) (AMP VS. CON)
acnB
icd
oorA
oorB
oorC
oorD
sucC
sucD
frdA
frdB
frdC
sdhA
sdhB
sdhC
fumC
mdh
mqo
gltA
Aconitase
Isocitrate dehydrogenase
α-ketoglutarate dehydrogenase
Succinyl-CoA synthetase
Succinic dehydrogenase
Fumarase
Malate dehydrogenase
Citrate synthase
b
mRNA
Protein
Fold change (log2) (AMP VS. CON)
accA
accB
accC
accD
fabD
fabH
fabG
fabZ
fabI
fabF
Initiation
Elongation
c
RNA
Protein
Fold change (log2) (AMP VS. CON)
Ferredoxin
Flavodoxin
Ferritin
d
mRNA
Protein
Fold change (log2) (CIP VS. CON)
e
mRNA
Protein
Fold change (log2) (CIP VS. CON)
f
RNA
Protein
Fold change (log2) (CIP VS. CON)
g
Complex I
Complex II
Complex III
Complex IV
Complex V
mRNA
Protein
Not detected proteins
Fold change (log2) (AMP VS. CON)
nuoA
nuoB
nuoC
nuoD
nuoE
nuoF
nuoG
nuoH
nuoI
nuoJ
nuoK
nuoL
nuoM
nuoN
sdhA
sdhB
sdhC
frdA
frdB
frdC
petA
petB
petC
ccoP
ccoO
ccoQ
ccoN
cydA
cydB
atpA
atpB
atpC
atpD
atpE
atpF
atpG
atpH
ppk
ppa
h
Complex I
Complex II
Complex III
Complex IV
Complex V
mRNA
Protein
Not detected proteins
Fold change (log2) (CIP VS. CON)

772

773 **Extended Data Figure 2. Transcriptomic and proteomic remodeling of central metabolism,**
774 **fatty acid biosynthesis, redox-associated factors and respiratory complexes in antibiotic-**
775 **tolerant *C. jejuni*.** (a, b) Log2 fold changes in mRNA and protein abundance of selected
776 tricarboxylic acid (TCA) cycle and associated metabolic enzymes in ampicillin (AMP)-selected
777 (a) and ciprofloxacin (CIP)-selected (b) tolerant cells relative to untreated control cells (CON).
778 (c, d) Log2 fold changes in mRNA and protein abundance of selected fatty acid biosynthesis
779 enzymes in AMP-selected (c) and CIP-selected (d) tolerant cells relative to untreated controls.
780 (e, f) Log2 fold changes in mRNA and protein abundance of selected redox- and iron-associated
781 factors, including ferredoxin, flavodoxin and ferritin, in AMP-selected (e) and CIP-selected (f)
782 tolerant cells relative to untreated controls.
783 (g, h) Log2 fold changes in mRNA and protein abundance of subunits of respiratory complexes
784 I–V in AMP-selected (g) and CIP-selected (h) tolerant cells relative to untreated controls. Red,
785 mRNA; blue, protein. Black dots indicate proteins not detected in the proteomic dataset. Features
786 detected exclusively by transcriptomics, with no corresponding detection in the proteomics, are
787 annotated as -∞ fold change for visualization purposes.

788

789

790

REFERENCES

1. Bigger, J., *Treatment of Staphylococcal Infections with Penicillin by Intermittent Sterilisation.* 1944.
2. Balaban, N.Q., S. Helaine, K. Lewis, M. Ackermann, B. Aldridge, D.I. Andersson, M.P. Brynildsen, D. Bumann, A. Camilli, and J.J. Collins, *Definitions and guidelines for research on antibiotic persistence.* Nature Reviews Microbiology, 2019. **17**(7): p. 441-448.
3. Fisher, R.A., B. Gollan, and S. Helaine, *Persistent bacterial infections and persister cells.* Nature Reviews Microbiology, 2017. **15**(8): p. 453-464.
4. Bloomfield, S.J., A.C. Midwinter, P.J. Biggs, N.P. French, J.C. Marshall, D.T. Hayman, P.E. Carter, C. Thornley, R. Yap, and J. Benschop, *Long-term colonization by Campylobacter jejuni within a human host: evolution, antimicrobial resistance, and adaptation.* The Journal of Infectious Diseases, 2018. **217**(1): p. 103-111.
5. Claudi, B., P. Spröte, A. Chirkova, N. Personnic, J. Zankl, N. Schürmann, A. Schmidt, and D. Bumann, *Phenotypic variation of Salmonella in host tissues delays eradication by antimicrobial chemotherapy.* Cell, 2014. **158**(4): p. 722-733.
6. Balaban, N.Q., J. Merrin, R. Chait, L. Kowalik, and S. Leibler, *Bacterial persistence as a phenotypic switch.* Science, 2004. **305**(5690): p. 1622-1625.
7. Balaban, N.Q., K. Gerdes, K. Lewis, and J.D. McKinney, *A problem of persistence: still more questions than answers?* Nature Reviews Microbiology, 2013. **11**(8): p. 587-591.
8. Lopatkin, A.J., J.M. Stokes, E.J. Zheng, J.H. Yang, M.K. Takahashi, L. You, and J.J. Collins, *Bacterial metabolic state more accurately predicts antibiotic lethality than growth rate.* Nature microbiology, 2019. **4**(12): p. 2109-2117.
9. Niu, H., J. Gu, and Y. Zhang, *Bacterial persisters: molecular mechanisms and therapeutic development.* Signal transduction and targeted therapy, 2024. **9**(1): p. 174.
10. Horak, R.D., J.A. Ciemniecki, and D.K. Newman, *Bioenergetic suppression by redox-active metabolites promotes antibiotic tolerance in Pseudomonas aeruginosa.* Proceedings of the National Academy of Sciences, 2024. **121**(46): p. e2406555121.
11. Sies, H., R.J. Mailloux, and U. Jakob, *Fundamentals of redox regulation in biology.* Nature Reviews Molecular Cell Biology, 2024. **25**(9): p. 701-719.
12. Dwyer, D.J., P.A. Belenky, J.H. Yang, I.C. MacDonald, J.D. Martell, N. Takahashi, C.T. Chan, M.A. Lobritz, D. Braff, and E.G. Schwarz, *Antibiotics induce redox-related physiological alterations as part of their lethality.* Proceedings of the National Academy of Sciences, 2014. **111**(20): p. E2100-E2109.
13. Baquero, F. and B.R. Levin, *Proximate and ultimate causes of the bactericidal action of antibiotics.* Nature Reviews Microbiology, 2021. **19**(2): p. 123-132.
14. Ahmad, M., S.V. Aduru, R.P. Smith, Z. Zhao, and A.J. Lopatkin, *The role of bacterial metabolism in antimicrobial resistance.* Nature Reviews Microbiology, 2025. **23**(7): p. 439-454.
15. Zheng, E.J., I.W. Andrews, A.T. Grote, A.L. Manson, M.A. Alcantar, A.M. Earl, and J.J. Collins, *Modulating the evolutionary trajectory of tolerance using antibiotics with different metabolic dependencies.* Nature Communications, 2022. **13**(1): p. 2525.
16. Kohanski, M.A., D.J. Dwyer, B. Hayete, C.A. Lawrence, and J.J. Collins, *A common mechanism of cellular death induced by bactericidal antibiotics.* Cell, 2007. **130**(5): p. 797-810.

17. Van den Bergh, B., M. Fauvart, and J. Michiels, *Formation, physiology, ecology, evolution and clinical importance of bacterial persisters.* FEMS microbiology reviews, 2017. **41**(3): p. 219-251.
18. Conlon, B.P., S.E. Rowe, A.B. Gandt, A.S. Nuxoll, N.P. Donegan, E.A. Zalis, G. Clair, J.N. Adkins, A.L. Cheung, and K. Lewis, *Persister formation in Staphylococcus aureus is associated with ATP depletion.* Nature microbiology, 2016. **1**(5): p. 16051.
19. Shan, Y., A. Brown Gandt, S. Rowe, J. Deisinger, B. Conlon, and K. Lewis, *ATP-dependent persister formation in Escherichia coli. MBio. 2017; 8 (1): e02267–16.* Article PubMed PubMed Central.
20. Amato, S.M., M.A. Orman, and M.P. Brynildsen, *Metabolic control of persister formation in Escherichia coli.* Molecular cell, 2013. **50**(4): p. 475-487.
21. Dewachter, L., C. Bollen, D. Wilmaerts, E. Louwagie, P. Herpels, P. Matthay, L. Khodaparast, L. Khodaparast, F. Rousseau, and J. Schymkowitz, *The dynamic transition of persistence toward the viable but nonculturable state during stationary phase is driven by protein aggregation.* MBio, 2021. **12**(4): p. 10.1128/mbio. 00703-21.
22. Pu, Y., Y. Li, X. Jin, T. Tian, Q. Ma, Z. Zhao, S.-y. Lin, Z. Chen, B. Li, and G. Yao, *ATP-dependent dynamic protein aggregation regulates bacterial dormancy depth critical for antibiotic tolerance.* Molecular cell, 2019. **73**(1): p. 143-156. e4.
23. Schramm, F.D., K. Schroeder, and K. Jonas, *Protein aggregation in bacteria.* FEMS microbiology reviews, 2020. **44**(1): p. 54-72.
24. Govers, S.K., E. Gayan, and A. Aertsen, *Intracellular movement of protein aggregates reveals heterogeneous inactivation and resuscitation dynamics in stressed populations of Escherichia coli.* Environmental microbiology, 2017. **19**(2): p. 511-523.
25. Wagener, L., A. Nath, M. Tuğrul, A. Aertsen, U.K. Steiner, and A.M. Proenca, *Protein aggregation drives cell aging in a size-specific manner in Escherichia coli.* Mbio, 2026. **17**(1): p. e02050-25.
26. Li, Y., X. Chen, W. Zhang, K. Fang, J. Tian, F. Li, M. Han, J. Huang, T. Sun, and F. Bai, *The metabolic slowdown caused by the deletion of pspA accelerates protein aggregation during stationary phase facilitating antibiotic persistence.* Antimicrobial Agents and Chemotherapy, 2024. **68**(2): p. e00937-23.
27. Page, R. and W. Peti, *Toxin-antitoxin systems in bacterial growth arrest and persistence.* Nature chemical biology, 2016. **12**(4): p. 208-214.
28. Tripathi, A., P.C. Dewan, S. Ahmed, and R. Varadarajan, *MazF-induced growth inhibition and persister generation in Escherichia coli.* Journal of Biological chemistry, 2014. **289**(7): p. 4191-4205.
29. Goormaghtigh, F., N. Fraikin, M. Putrinš, T. Hallaert, V. Hauryliuk, A. Garcia-Pino, A. Sjödin, S. Kasvandik, K. Udekwu, and T. Tenson, *Reassessing the role of type II toxin-antitoxin systems in formation of Escherichia coli type II persister cells.* MBio, 2018. **9**(3): p. 10.1128/mbio. 00640-18.
30. Leinberger, F.H., L. Cassidy, D. Edelmann, N.E. Schmid, M. Oberpaul, P. Blumenkamp, S. Schmidt, A. Natriashvili, M.H. Ulbrich, and A. Tholey, *Protein aggregation is a consequence of the dormancy-inducing membrane toxin TisB in Escherichia coli.* Msystems, 2024. **9**(11): p. e01060-24.
31. Cayron, J., T. Oms, T. Schlechtweg, S. Zedek, and L. Van Melderen, *TisB protein is the single molecular determinant underlying multiple downstream effects of ofloxacin in Escherichia coli.* Science Advances, 2024. **10**(13): p. eadk1577.

32. Keren, I., Y. Wu, J. Inocencio, L.R. Mulcahy, and K. Lewis, *Killing by bactericidal antibiotics does not depend on reactive oxygen species.* Science, 2013. **339**(6124): p. 1213-1216.
33. Liu, Y. and J.A. Imlay, *Cell death from antibiotics without the involvement of reactive oxygen species.* Science, 2013. **339**(6124): p. 1210-1213.
34. Lobritz, M.A., P. Belenky, C.B. Porter, A. Gutierrez, J.H. Yang, E.G. Schwarz, D.J. Dwyer, A.S. Khalil, and J.J. Collins, *Antibiotic efficacy is linked to bacterial cellular respiration.* Proceedings of the National Academy of Sciences, 2015. **112**(27): p. 8173-8180.
35. Dwyer, D.J., J.J. Collins, and G.C. Walker, *Unraveling the physiological complexities of antibiotic lethality.* Annual review of pharmacology and toxicology, 2015. **55**(1): p. 313-332.
36. Van Acker, H. and T. Coenye, *The role of reactive oxygen species in antibiotic-mediated killing of bacteria.* Trends in microbiology, 2017. **25**(6): p. 456-466.
37. Parkhill, J., B. Wren, K. Mungall, J. Ketley, C. Churcher, D. Basham, T. Chillingworth, R. Davies, T. Feltwell, and S. Holroyd, *The genome sequence of the food-borne pathogen Campylobacter jejuni reveals hypervariable sequences.* Nature, 2000. **403**(6770): p. 665-668.
38. Pearson, B.M., D.J. Gaskin, R.P. Segers, J.M. Wells, P.J. Nuijten, and A.H. Van Vliet, *The complete genome sequence of Campylobacter jejuni strain 81116 (NCTC11828).* Journal of bacteriology, 2007. **189**(22): p. 8402-8403.
39. Ovsepian, A., M.H. Larsen, C.S. Vegge, and H. Ingmer, *Ciprofloxacin-induced persister-cells in Campylobacter jejuni.* Microbiology, 2020. **166**(9): p. 849-853.
40. Morcrette, H., A. Kovacs-Simon, R.K. Tennant, J. Love, S. Wagley, Z.R. Yang, D.J. Studholme, O.S. Soyer, O.L. Champion, and C.S. Butler, *Campylobacter jejuni 11168H exposed to penicillin forms persister cells and cells with altered redox protein activity.* Frontiers in Cellular and Infection Microbiology, 2020. **10**: p. 565975.
41. Park, M., J. Kim, J. Feinstein, K.S. Lang, S. Ryu, and B. Jeon, *Development of fluoroquinolone resistance through antibiotic tolerance in Campylobacter jejuni.* Microbiology Spectrum, 2022. **10**(5): p. e01667-22.
42. Gaynor, E.C., D.H. Wells, J.K. MacKichan, and S. Falkow, *The Campylobacter jejuni stringent response controls specific stress survival and virulence-associated phenotypes.* Molecular microbiology, 2005. **56**(1): p. 8-27.
43. Gaasbeek, E.J., F.J. van der Wal, J.P. van Putten, P. de Boer, L. van der Graaf-van Bloois, A.G. de Boer, B.J. Vermaning, and J.A. Wagenaar, *Functional characterization of excision repair and RecA-dependent recombinational DNA repair in Campylobacter jejuni.* Journal of bacteriology, 2009. **191**(12): p. 3785-3793.
44. Bittner, L.M., J. Arends, and F. Narberhaus, *Mini review: ATP-dependent proteases in bacteria.* Biopolymers, 2016. **105**(8): p. 505-517.
45. Meng, F. and L. Kurgan, *DFLpred: High-throughput prediction of disordered flexible linker regions in protein sequences.* Bioinformatics, 2016. **32**(12): p. i341-i350.
46. Gsponer, J. and M.M. Babu, *Cellular strategies for regulating functional and nonfunctional protein aggregation.* Cell reports, 2012. **2**(5): p. 1425-1437.
47. Taylor, A.J. and D.J. Kelly, *The function, biogenesis and regulation of the electron transport chains in Campylobacter jejuni: new insights into the bioenergetics of a major food-borne pathogen.* Advances in microbial physiology, 2019. **74**: p. 239-329.

48. Jackson, R.J., K.T. Elvers, L.J. Lee, M.D. Gidley, L.M. Wainwright, J. Lightfoot, S.F. Park, and R.K. Poole, *Oxygen reactivity of both respiratory oxidases in Campylobacter jejuni: the cydAB genes encode a cyanide-resistant, low-affinity oxidase that is not of the cytochrome bd type.* Journal of bacteriology, 2007. **189**(5): p. 1604-1615.
49. Borisov, V.B., S.A. Siletsky, M.R. Nastasi, and E. Forte, *ROS defense systems and terminal oxidases in bacteria.* Antioxidants, 2021. **10**(6): p. 839.
50. de Geus, P., I. van Die, H. Bergmans, J. Tommassen, and G. de Haas, *Molecular cloning of pldA, the structural gene for outer membrane phospholipase of E. coli K12.* Molecular and General Genetics MGG, 1983. **190**: p. 150-155.
51. Wright, G.C., J. Weiss, K.S. Kim, H. Verheij, and P. Elsbach, *Bacterial phospholipid hydrolysis enhances the destruction of Escherichia coli ingested by rabbit neutrophils. Role of cellular and extracellular phospholipases.* The Journal of clinical investigation, 1990. **85**(6): p. 1925-1935.
52. Stahl, M., J. Ries, J. Vermeulen, H. Yang, H.P. Sham, S.M. Crowley, Y. Badayeva, S.E. Turvey, E.C. Gaynor, and X. Li, *A novel mouse model of Campylobacter jejuni gastroenteritis reveals key pro-inflammatory and tissue protective roles for Toll-like receptor signaling during infection.* PLoS pathogens, 2014. **10**(7): p. e1004264.
53. Bhusal, R.P., J.J. Barr, and D. Subedi, *A metabolic perspective into antimicrobial tolerance and resistance.* The Lancet Microbe, 2022. **3**(3): p. e160-e161.
54. Meylan, S., I.W. Andrews, and J.J. Collins, *Targeting antibiotic tolerance, pathogen by pathogen.* Cell, 2018. **172**(6): p. 1228-1238.
55. Liu, J., O. Gefen, I. Ronin, M. Bar-Meir, and N.Q. Balaban, *Effect of tolerance on the evolution of antibiotic resistance under drug combinations.* Science, 2020. **367**(6474): p. 200-204.
56. Orman, M.A., H.G. Ngo, and S.G. Mohiuddin, *Beyond metabolic dormancy: metabolic rewiring in bacterial persistence.* Nature Communications, 2026. **17**(1): p. 3536.
57. Gaillot, O., E. Pellegrini, S. Bregenholt, S. Nair, and P. Berche, *The ClpP serine protease is essential for the intracellular parasitism and virulence of Listeria monocytogenes.* Molecular microbiology, 2000. **35**(6): p. 1286-1294.
58. Frees, D., S.N. Qazi, P.J. Hill, and H. Ingmer, *Alternative roles of ClpX and ClpP in Staphylococcus aureus stress tolerance and virulence.* Molecular microbiology, 2003. **48**(6): p. 1565-1578.
59. Feng, J., S. Michalik, A.N. Varming, J.H. Andersen, D. Albrecht, L. Jelsbak, S. Krieger, K. Ohlsen, M. Hecker, and U. Gerth, *Trapping and proteomic identification of cellular substrates of the ClpP protease in Staphylococcus aureus.* Journal of proteome research, 2013. **12**(2): p. 547-558.
60. Alqarzaee, A.A., S.S. Chaudhari, M.M. Islam, V. Kumar, M.C. Zimmerman, R. Saha, K.W. Bayles, D. Frees, and V.C. Thomas, *Staphylococcal ClpXP protease targets the cellular antioxidant system to eliminate fitness-compromised cells in stationary phase.* Proceedings of the National Academy of Sciences, 2021. **118**(47): p. e2109671118.
61. Flynn, J.M., S.B. Neher, Y.-I. Kim, R.T. Sauer, and T.A. Baker, *Proteomic discovery of cellular substrates of the ClpXP protease reveals five classes of ClpX-recognition signals.* Molecular cell, 2003. **11**(3): p. 671-683.
62. Ghanbarpour, A., R.T. Sauer, and J.H. Davis, *A proteolytic AAA+ machine poised to unfold protein substrates.* Nature communications, 2024. **15**(1): p. 9681.

63. Culp, E. and G.D. Wright, *Bacterial proteases, untapped antimicrobial drug targets.* The Journal of antibiotics, 2017. **70**(4): p. 366-377.
64. Basta, D.W., D. Angeles-Albores, M.A. Spero, J.A. Ciemniecki, and D.K. Newman, *Heat-shock proteases promote survival of Pseudomonas aeruginosa during growth arrest.* Proceedings of the National Academy of Sciences, 2020. **117**(8): p. 4358-4367.
65. Huemer, M., S. Mairpady Shambat, J. Bergada-Pijuan, S. Söderholm, M. Boumasmoud, C. Vulin, A. Gómez-Mejia, M. Antelo Varela, V. Tripathi, and S. Götschi, *Molecular reprogramming and phenotype switching in Staphylococcus aureus lead to high antibiotic persistence and affect therapy success.* Proceedings of the National Academy of Sciences, 2021. **118**(7): p. e2014920118.
66. Fung, D.K., J.T. Barra, J. Yang, J.W. Schroeder, F. She, M. Young, D. Ying, D.M. Stevenson, D. Amador-Noguez, and J.D. Wang, *A shared alarmone–GTP switch controls persister formation in bacteria.* Nature Microbiology, 2025. **10**(7): p. 1617-1629.
67. Ciemniecki, J.A., C.-L. Ho, R.D. Horak, A. Okamoto, and D.K. Newman, *Mechanistic study of a low-power bacterial maintenance state using high-throughput electrochemistry.* Cell, 2024. **187**(24): p. 6882-6895. e8.
68. Shiraliyev, R. and M.A. Orman, *Metabolic disruption impairs ribosomal protein levels, resulting in enhanced aminoglycoside tolerance.* Elife, 2024. **13**: p. RP94903.
69. Patel, A., D. McGrosso, Y. Hefner, A. Campeau, A.V. Sastry, S. Maurya, K. Rychel, D.J. Gonzalez, and B.O. Palsson, *Proteome allocation is linked to transcriptional regulation through a modularized transcriptome.* Nature Communications, 2024. **15**(1): p. 5234.
70. Zhang, M., C. Zhang, A. Ramos, R.J. Whitaker, and M. Whiteley, *Conserved cross-domain protein-to-mRNA ratios enable proteome prediction in microbes.* Mbio, 2025. **16**(8): p. e01411-25.
71. Bexley, K., M. Ristová, S. Sharma, C. Spanos, A. Chabes, and D. Tollervey, *Rapid remodeling of NTP levels enables immediate translational adaptation to energy stress in yeast.* Molecular cell, 2025. **85**(19): p. 3623-3639. e7.
72. Froschauer, K., S.L. Svensson, R. Gelhausen, E. Fiore, P. Kible, A. Klaude, M. Kucklick, S. Fuchs, F. Eggenhofer, and C. Yang, *Complementary Ribo-seq approaches map the translatome and provide a small protein census in the foodborne pathogen Campylobacter jejuni.* Nature Communications, 2025. **16**(1): p. 3078.
73. Aldikacti, B., H. Putun, V. Sarsani, R. Zeinert, P. Flaherty, and P. Chien, *Stress testing reveals selective vulnerabilities in protein homeostasis.* Cell Reports, 2026. **45**(2).
74. Sass, P., M. Josten, K. Famulla, G. Schiffer, H.-G. Sahl, L. Hamoen, and H. Brötz-Oesterhelt, *Antibiotic acyldepsipeptides activate ClpP peptidase to degrade the cell division protein FtsZ.* Proceedings of the National Academy of Sciences, 2011. **108**(42): p. 17474-17479.
75. Labana, P., M.H. Dornan, M. Lafrenière, T.L. Czarny, E.D. Brown, J.P. Pezacki, and C.N. Boddy, *Armeniaspirols inhibit the AAA+ proteases ClpXP and ClpYQ leading to cell division arrest in Gram-positive bacteria.* Cell Chemical Biology, 2021. **28**(12): p. 1703-1715. e11.
76. Bollen, C., S. Louwagie, F. Deroover, W. Duverger, L. Khodaparast, L. Khodaparast, D. Hofkens, J. Schymkowitz, F. Rousseau, and L. Dewachter, *Composition and liquid-to-solid maturation of protein aggregates contribute to bacterial dormancy development and recovery.* Nature communications, 2025. **16**(1): p. 1046.

1018 77. Sniezek, K.J., N. Soto-Echevarria, and M.P. Brynildsen, *Solidification of protein*
1019 *aggregates deepens bacterial dormancy.* Trends in Microbiology, 2025.
1020 78. Lodhiya, T., A. Palande, A. Veeram, G.J. Larrouy-Maumus, D.J. Beste, and R.
1021 Mukherjee, *ATP burst is the dominant driver of antibiotic lethality in Mycobacterium*
1022 *smegmatis.* ELife, 2026. **13**: p. RP99656.
1023 79. Borrelli, C., E.J. Douglas, S.M. Riley, A.E. Lemonidi, G. Larrouy-Maumus, W.-J. Lu,
1024 B.B. Bonev, A.M. Edwards, and B.W. Hoogenboom, *Polymyxin B lethality requires*
1025 *energy-dependent outer membrane disruption.* Nature Microbiology, 2025. **10**(11): p.
1026 2919-2933.
1027 80. Li, B., S. Srivastava, M. Shaikh, G. Mereddy, M.R. Garcia, E.N. Chiles, A. Shah, B.
1028 Ofori-Anyinam, T.-Y. Chu, and N.J. Cheney, *Bioenergetic stress potentiates antimicrobial*
1029 *resistance and persistence.* Nature communications, 2025. **16**(1): p. 5111.
1030 81. Ofori-Anyinam, B., M. Hamblin, M.L. Coldren, B. Li, G. Mereddy, M. Shaikh, A. Shah,
1031 C. Grady, N. Ranu, and S. Lu, *Catalase activity deficiency sensitizes multidrug-resistant*
1032 *Mycobacterium tuberculosis to the ATP synthase inhibitor bedaquiline.* Nature
1033 communications, 2024. **15**(1): p. 9792.
1034 82. Kalia, N.P., S. Singh, K. Hards, C.-Y. Cheung, E. Sviriaeva, A. Banaei-Esfahani, R.
1035 Aebersold, M. Berney, G.M. Cook, and K. Pethe, *M. tuberculosis relies on trace oxygen*
1036 *to maintain energy homeostasis and survive in hypoxic environments.* Cell Reports, 2023.
1037 **42**(5).
1038 83. Weingarten, R.A., J.L. Grimes, and J.W. Olson, *Role of Campylobacter jejuni respiratory*
1039 *oxidases and reductases in host colonization.* Applied and environmental microbiology,
1040 2008. **74**(5): p. 1367-1375.
1041 84. Seregina, T., R. Shakulov, G. Quarta, K. Shatalin, S. Sklyarova, I. Petrushanko, A.P.
1042 Fedulov, A.V. Ivanov, V. Mitkevich, and A. Makarov, *Ribose-5-phosphate metabolism*
1043 *protects E. coli from antibiotic lethality.* mBio, 2025. **16**(8): p. e00654-25.
1044 85. Gray, D.A., B. Wang, M. Sidarta, F.A. Cornejo, J. Wijnheijmer, R. Rani, P. Gamba, K.
1045 Turgay, M. Wenzel, and H. Strahl, *Membrane depolarization kills dormant Bacillus*
1046 *subtilis cells by generating a lethal dose of ROS.* Nature Communications, 2024. **15**(1): p.
1047 6877.
1048 86. Cao, X., C.H. van de Lest, L.Z. Huang, J.P. van Putten, and M.M. Wösten,
1049 *Campylobacter jejuni permeabilizes the host cell membrane by short chain*
1050 *lysophosphatidylethanolamines.* Gut Microbes, 2022. **14**(1): p. 2091371.
1051 87. Konkel, M.E., J.E. Christensen, A.S. Dhillon, A.B. Lane, R. Hare-Sanford, D.M.
1052 Schaberg, and C.L. Larson, *Campylobacter jejuni strains compete for colonization in*
1053 *broiler chicks.* Applied and environmental microbiology, 2007. **73**(7): p. 2297-2305.
1054 88. Cox, J., M.Y. Hein, C.A. Luber, I. Paron, N. Nagaraj, and M. Mann, *Accurate proteome-*
1055 *wide label-free quantification by delayed normalization and maximal peptide ratio*
1056 *extraction, termed MaxLFQ.* Molecular & cellular proteomics, 2014. **13**(9): p. 2513-
1057 2526.
1058 89. Galperin, M.Y., K.S. Makarova, Y.I. Wolf, and E.V. Koonin, *Expanded microbial genome*
1059 *coverage and improved protein family annotation in the COG database.* Nucleic acids
1060 research, 2015. **43**(D1): p. D261-D269.
1061 90. Reimand, J., R. Isserlin, V. Voisin, M. Kucera, C. Tannus-Lopes, A. Rostamianfar, L.
1062 Wadi, M. Meyer, J. Wong, and C. Xu, *Pathway enrichment analysis and visualization of*

1063 *omics data using g: Profiler, GSEA, Cytoscape and EnrichmentMap.* Nature protocols,
1064 2019. **14**(2): p. 482-517.
1065 91. Subramanian, A., P. Tamayo, V.K. Mootha, S. Mukherjee, B.L. Ebert, M.A. Gillette, A.
1066 Paulovich, S.L. Pomeroy, T.R. Golub, and E.S. Lander, *Gene set enrichment analysis: a*
1067 *knowledge-based approach for interpreting genome-wide expression profiles.*
1068 Proceedings of the National Academy of Sciences, 2005. **102**(43): p. 15545-15550.
1069 92. Cline, M.S., M. Smoot, E. Cerami, A. Kuchinsky, N. Landys, C. Workman, R. Christmas,
1070 I. Avila-Campilo, M. Creech, and B. Gross, *Integration of biological networks and gene*
1071 *expression data using Cytoscape.* Nature protocols, 2007. **2**(10): p. 2366.
1072 93. Buckner, M.M., L.C.M. Antunes, N. Gill, S.L. Russell, S.R. Shames, and B.B. Finlay, *15-*
1073 *Deoxy-Δ12, 14-prostaglandin J2 inhibits macrophage colonization by Salmonella*
1074 *enterica serovar Typhimurium.* PLoS One, 2013. **8**(7): p. e69759.

1075